ORNL/TM-2023/3072

Modeling Enhancements and Demonstration of Shift Capabilities for PBRs and MSRs

Tara Pandya
Tarek Ghaddar
Friederike Bostelmann
Matthew Jessee
Philip Britt

October 19, 2023

OAK RIDGE National Laboratory

ORNL IS MANAGED BY UT–BATTELLE, LLC, FOR THE U.S. DEPARTMENT OF ENERGY

ORNL/TM-2023/3072

Nuclear Energy and Fuel Cycle Division

MODELING ENHANCEMENTS AND DEMONSTRATION OF SHIFT CAPABILITIES FOR PBRS AND MSRS

Tara Pandya
Tarek Ghaddar
Friederike Bostelmann
Matthew Jessee
Philip Britt

October 19, 2023

Prepared by
OAK RIDGE NATIONAL LABORATORY
Oak Ridge, TN 37831-6283
managed by
UT-BATTELLE, LLC
for the
US DEPARTMENT OF ENERGY
under contract DE-AC05-00OR22725

CONTENTS

LIST OF FIGURES

LIST OF TABLES

LIST OF LISTINGS

ABBREVIATIONS

ABTR	Advanced Breeder Test Reactor
ANL	Argonne National Laboratory
API	application programming interface
BWR	boiling water reactor
CANDU	Canadian Deuterium Uranium
CE	continuous energy
CPU	central processing unit
CSAS	Criticality Safety Analysis Sequence
DEM	Discrete Element Method
DOE	Department of Energy
ENDF	Evaluated Nuclear Data File
FY	fiscal year
GPBR	generic pebble bed reactor
GU-EULA	Government-Use End Use License Agreement
HDF5	Hierarchical Data Format 5
INL	Idaho National Laboratory
LWR	light-water reactor
M&S	modeling and simulation
MC	Monte Carlo
MSR	molten salt reactor
MSRE	Molten Salt Reactor Experiment
NEAMS	Nuclear Energy Advanced Modeling and Simulation
ORANGE	Oak Ridge Adaptable Nested Geometry Engine
ORIGEN	Oak Ridge Isotope Generator
ORNL	Oak Ridge National Laboratory
PBR	pebble-bed reactor
TRISO	tristructural isotropic

ABSTRACT

This technical report documents the modeling enhancements and demonstrations with the Shift Monte Carlo (MC) code targeted at pebble-bed reactors (PBRs) and molten salt reactors (MSRs) under the US Department of Energy (DOE) Nuclear Energy Advanced Modeling and Simulation (NEAMS) program in fiscal year (FY) 2023. The work performed included several enhancements, such as improvements for multigroup cross section generation, a new eigenvalue mode considering only prompt fission neutrons, and enhancements to the Titan frontend for Shift to allow for new geometry types and tally functionality. Additionally, new PBR equilibrium core search reference calculations were generated with Shift and compared to Serpent calculations provided by Idaho National Laboratory (INL). These enhancements provide a robust foundation for applying Shift for both reference and two-step neutronics analysis for advanced reactor simulation.

1. INTRODUCTION

The US Department of Energy (DOE) Office of Nuclear Energy Nuclear Energy Advanced Modeling and Simulation (NEAMS) program develops advanced modeling and simulation (M&S) tools to accelerate the deployment of advanced nuclear energy technologies. The reactor physics technical area focuses on the development of M&S tools for modeling reactor physics phenomena (i.e., neutral particle transport and isotopic depletion/decay). The three primary codes supported in the reactor physics technical area are Griffin for non–light-water reactor (LWR) reactor physics, MPACT for LWR reactor physics, and the Shift Monte Carlo (MC) code used for reference solutions, ex-core dose assessment, cross section generation, and sensitivity and uncertainty assessment.

This report presents the modeling enhancements, multigroup cross section enhancements, and a pebble-bed reactor (PBR) demonstration using Shift completed during fiscal year (FY)23. Modeling enhancements included the addition of new units, cell tallies, and a new tight packing fraction algorithm in Titan. Shift's multigroup cross section generation capabilities were extended to support calculation of energy deposition, neutron velocity, and kinetics parameters. Shift now also supports the ability to run a prompt eigenvalue calculation. Finally, the use of Shift for the generic pebble bed reactor (GPBR) equilibrium core search using *kugelpy* was demonstrated and is analyzed herein.

To allow for collaboration on beta releases of SCALE with NEAMS participants, the process of seeking SCALE's release under a Government-Use End Use License Agreement (GU-EULA) was undertaken in FY23. The GU-EULA was drafted and approved by Oak Ridge National Laboratory (ORNL). Per ORNL policy, this requires SCALE to follow US copyright procedure. The application for copyright is currently under review with the DOE Patent Council. Once approved, the institutional GU-EULA can be signed by the designated Idaho National Laboratory (INL) and Argonne National Laboratory (ANL) points of contact, and SCALE beta releases can then be controlled and accessible by NEAMS participants at each institution.

This report is organized as follows. Section 2 presents the enhancements and analysis of multigroup cross sections and parameters calculated by Shift targeting molten salt reactors (MSRs) and PBRs. Section 3 presents the modeling enhancements made to Titan targeting PBRs. Section 4.4 presents modeling enhancements for the GPBR and the demonstration of an equilibrium core search with Shift. Finally, Section 5 provides a summary of work completed in FY23 along with future development directions.

2. SHIFT MULTIGROUP CROSS SECTION ENHANCEMENTS

In FY23, the multigroup cross section generation capabilities of `Shift` were expanded and improved upon the FY22 implementation. All of these capabilities are available in `SCALE`7.0b6 (6/30/23), unless otherwise noted.

2.1 ISSUES FIXED

The following defects were found and fixed from the FY22 multigroup cross section generation implementation.

- An update was made to the scattering probability matrix and mean scattering angle tallying mechanics to properly account for secondary energy distributions. Since `Shift` accounts for these distributions by adjusting the weight of a particle after a collision occurs, this fix was a simple update to these tallies to use the post-collision particle weight for accumulation.
- An update was made in the generation of scattering matrices for homogenized cross section regions. The scattering matrix calculation synthesizes two separate tallies: a material-wise collision-based scattering probability matrix tally and a material-wise path length–based scattering tally. These two tallies were combined based on the user-defined cell union for the homogenization region of interest. The calculation allows for a different (potentially larger) cell union for the collision-based tally so as to reduce the tally variance without loss of accuracy. Further testing identified that this synthesis calculation had an error in processing the two different cell union sets. The previous workaround was to use the same cell union for both the collision-based and path length–based tallies, which requires more memory and produces cross section matrices with higher variance (this was the approach used in FY21 in [1]). This workaround is no longer required with `SCALE`7.0b6.
- An issue with improper sampling of probability tables in the unresolved resonance region for certain nuclides was resolved when tallying disappearance reactions. This issue was found when comparing analytic and `Shift`-generated eigenvalues and multigroup cross sections of a simple fast spectrum problem (i.e., an infinite homogeneous medium of UO_2). This issue was not previously realized when analyzing thermal systems because fast systems exacerbate this issue.

  Instead of directly tallying the total reaction rate using Evaluated Nuclear Data File (ENDF) MT=1, the *CELLNODAL* tallies in `Shift` tally the multiple reactions contributing to the total reaction as follows:

  $$RR_{\text{total}} = RR_{\text{fission}} + RR_{\text{absorption}} + RR_{1\text{N}} + RR_{2\text{N}} + RR_{3\text{N}} + RR_{4\text{N}}, \quad (1)$$

  where RR is the reaction rate. This is done because these reactions are also needed to produce other multigroup cross sections.

  Using the simple analytic test problem mentioned above, very-fine-group nuclide total reaction rate tallies were calculated with `Shift` by directly tallying MT=1 and by performing the summation shown in Eq. 1, both with and without probability table data sampling enabled. Figure 1 shows the U^{236} total reaction rate relative differences between these tallies, which clearly shows that probability table data are not being sampled properly in the unresolved resonance region. When tallying the absorption reaction rate, `Shift` previously used the data from MT=101 (N_DISAP), which is a summation of constituent MT values. It was incorrectly assumed that because some of these constituents contained probability table data on the continuous energy (CE) data files, MT=101 did as well. However, it was found that MT=101 stored only an average value on the CE data files.

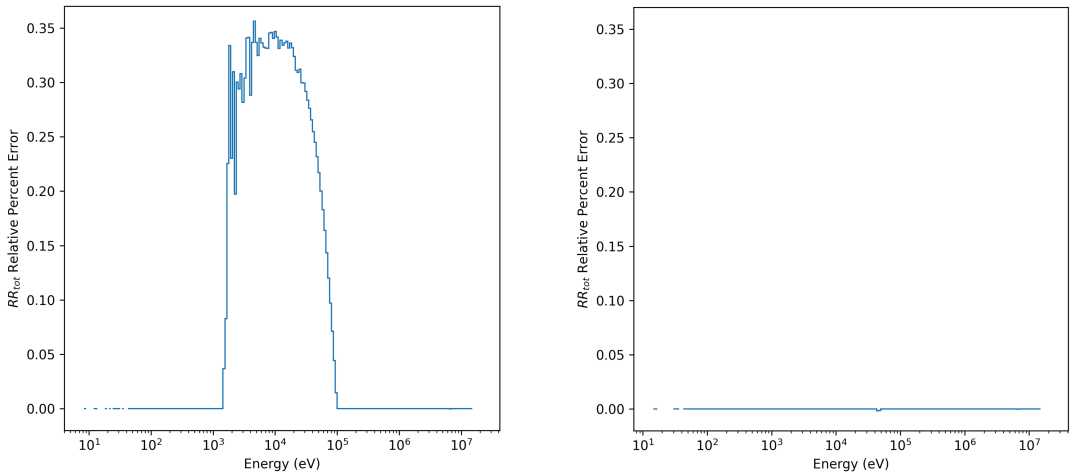

(a) With probability table sampling enabled **(b) Without probability table sampling enabled**

Figure 1. Infinite homogeneous medium U^{236} total reaction rate comparison.

Updating the absorption reaction rate to use a summation of MT=102–117 (the constituents of MT=101) led to agreement of the analytic and simulated k_{eff} for the simple infinite homogeneous medium test problem, as shown in Fig. 2. This figure shows convergence of k_{eff} as the number of particle histories is increased for three cases: the `Shift` calculated k_{eff}, the analytically calculated k_{eff} using multigroup cross sections from the updated *CELLNODAL* tally, and the analytically calculated k_{eff} using multigroup cross sections from a *MESHNODAL* tally that directly tallies MT=1 to obtain the total reaction rate. Note that multiple instances for each set of particle histories were run in order to get an estimate of the variance of the analytically calculated k_{eff} since `Shift` does not report variance of the multigroup cross sections. With this fix, all of these cases tend toward the same k_{eff} as particle histories increase.

- The default output units of κ_{fission} in the ISOXML file were updated from MeV to Joules to correspond to the default `Griffin` units. The κ_{fission} reaction rate and multigroup parameter output in the Hierarchical Data Format 5 (HDF5) output file still have units of MeV.

2.2 NEW CAPABILITIES

The following new capabilities were added to `Shift` for general advanced reactor analysis.

1. The ability to read κ values from an external HDF5 file was added. This capability allows the user to provide their own κ values. If an external file is not specified, then the pre-generated values in the **kappa.h5** `SCALE` data are used. The κ values on this file are taken from ENDF/B-IV and the reference by Kim et al [2, 3]. An example of how to specify a user-given file is shown in Listing 1.

Listing 1. Example Shift specification of external *kappa_library*.

```
[PHYSICS=sce]
ce_lib ce
mode n
kappa_library "path_to_data\my_kappas.h5"
```

The structure of this file must adhere to the expected `SCALE` κ data format. Therefore, a simple utility called *make-kappa-hdf5* has been provided to aid users in creating this file. This utility is included with a `SCALE`7.0b6 install, and the usage is shown below.

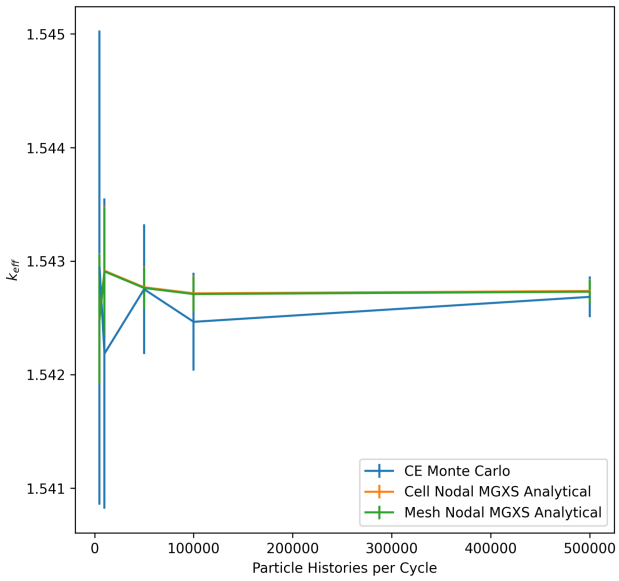

Figure 2. Infinite homogeneous medium k_{eff} convergence comparison.

```
usage: make-kappa-hdf5 [-h] [--version] [-g] [-c] [-v] [-q]
         [--very-quiet] [--silent]
         [--log {None,DEBUG,STATUS,INFO,WARNING,ERROR,CRITICAL}]
         [-e ENV]
         [--old_kappa_file OLD_KAPPA_FILE] --output OUTPUT
         [--fission_zaids FISSION_ZAIDS [FISSION_ZAIDS ...]]
         [--fission_kappas FISSION_KAPPAS [FISSION_KAPPAS ...]]
         [--capture_zaids CAPTURE_ZAIDS [CAPTURE_ZAIDS ...]]
         [--capture_kappas CAPTURE_KAPPAS [CAPTURE_KAPPAS ...]]
         [--default_fission_kappa DEFAULT_FISSION_KAPPA]
         [--default_capture_kappa DEFAULT_CAPTURE_KAPPA]
```

An example use of this conversion utility is to perform the following command.

```
make-kappa-hdf5
     --output test.h5
     --fission_zaids 8888 9999
     --fission_kappas 200.0 214.0
     --capture_zaids 1111 2222 8888
     --capture_kappas 5.1 5.4 5.7
```

2. The ability to tally and output the energy deposition per specified region was added. This tally is automatically enabled for a *CELLNODAL* tally (if the data are available) and is calculated for a given homogenized region and group, g, by

$$\kappa^g = \Sigma^g_{\text{fission}} \kappa_{\text{fission}} + \Sigma^g_{\text{capture}} \kappa_{\text{capture}}, \tag{2}$$

where Σ is the macroscopic cross section. The κ_{fission} and κ_{capture} values used for this tally are taken from the user-specified or default κ file described in item 1. The units of this tally in the HDF5 output file are in MeV, but the units in the post-processed ISOXML file are in Joules.

The following new capabilities were added for MSR modeling.

1. The ability to tally and output forward flux–weighted kinetics parameters ($\overline{\beta}, \overline{\lambda}$) with the *CELLNODAL* tally was added. This capability is automatically enabled if the **kinetics.h5** file is available and can be loaded from the `SCALE` CE data location. This data file contains delayed neutron fractions, total delayed neutron fractions, and delayed neutron decay constants for ^{232}Th, ^{233}U, ^{235}U, ^{238}U, ^{239}Pu, ^{240}Pu, and ^{241}Pu. The delayed neutron fractions and delayed neutron decay constants for a nuclide are given for the thermal and fast range for six delayed neutron precursors. The total delayed neutron fraction is given for the thermal and fast range for each nuclide. The user cannot currently provide their own kinetics data file.

   There are two new input parameters available to turn off the loading and calculation of these kinetics parameters. To turn off loading of the kinetics data file, the user simply sets the *kinetics* parameter in the *PHYSICS* block to "false" as shown in Listing 2. To turn off only the calculation of kinetics parameters in the *CELLNODAL* tally (but still allow the kinetics data to be loaded), the user can set the *calculate_kinetics* parameters to false, as shown in Listing 3.

Listing 2. Example Shift input to disable loading of kinetics data.

```
[PHYSICS=sce]
kinetics false
```

   If the calculation of kinetics parameters is enabled, then `Shift` produces $\overline{\beta}$ and $\overline{\lambda}$ values for each homogenized region for six delayed neutron precursor groups. The average delayed neutron fraction for a precursor group is calculated as

$$\overline{\beta_i} = \frac{\sum_n \sum_j \alpha_{n,i,j} \int_{E_j}^{E_{j+1}} \nu_{d,n}(E)\,\Sigma_{f,n}(E)\,\phi(E)}{\sum_j \int_{E_j}^{E_{j+1}} \nu(E)\,\Sigma_f(E)\,\phi(E)}, \tag{3}$$

   and the average delayed neutron precursor decay constant is calculated as

$$\overline{\lambda_i} = \frac{\sum_n \sum_j \alpha_{n,i,j} \int_{E_j}^{E_{j+1}} \nu_{d,n}(E)\,\Sigma_{f,n}(E)\,\phi(E)}{\sum_n \sum_j \frac{\alpha_{n,i,j}}{\lambda_{n,i,j}} \int_{E_j}^{E_{j+1}} \nu_{d,n}(E)\,\Sigma_{f,n}(E)\,\phi(E)}, \tag{4}$$

   where i is the precursor group index, n is the nuclide index, j is the energy group index, $\nu_{d,n}$ is the average number of delayed neutrons emitted per nuclide fission, and

$$\alpha_{n,i,j} = \frac{\beta_{n,i,j}}{\beta_{n,total,j}}. \tag{5}$$

   As previously stated, the values for $\beta_{n,i,j}$, $\beta_{n,total,j}$, and $\lambda_{n,i,j}$ are from the **kinetics.h5** data for each nuclide. See the book by Cacuci for further derivation details [4].

   Besides being written to the `Shift` HDF5 output file, the delayed neutron fractions and delayed neutron precursors decay constants are written to the ISOXML file as the *DNFraction* and *DNPlamda*. `Shift` does not currently calculate the delayed neutron spectrum. This is an area for

future work. For each homogenized region, the value for the total fission spectrum is also written for the delayed neutron spectrum (*DNSpectrum*) for the six delayed neutron precursor groups on the ISOXML file. Future work to produce adjoint flux–weighted kinetics parameters with `Shift` is needed to potentially achieve better accuracy.

Listing 3. Example Shift input to disable calculation of kinetics parameters.

```
[TALLY][CELLNODAL example]
calculate_kinetics false
```

2. Calculation and output of the multigroup velocity was added to the *CELLNODAL* tally (to be released in SCALE7.0b7 (9/30/23). This parameter is needed for transient deterministic calculations. `Shift` calculates velocity as a forward-weighted quantity as shown in Eq. 6.

$$1/V_G = \frac{\sum_g w_g \phi_g / v_g}{\sum_g w_g \phi_g} \tag{6}$$

where

$$v_g = \sqrt{\frac{2E_g}{m_n}},$$
$$w_g \approx 1,$$
$$E_g = \sqrt{E_g^{upper} E_g^{lower}},$$

and m_n is the mass of a neutron. The velocity is automatically calculated and output when a *CELLNODAL* tally is specified, and the units of velocity are output to the ISOXML file in cm/s.

3. The ability to perform prompt-only eigenvalue calculations with `Shift` was added in SCALE7.0b6 (06/30/23) with a bug fix update in SCALE7.0b7 (09/30/23). This capability allows for a simple estimate of β_{eff} that can be compared with the calculated β_{eff} from the *CELLNODAL* tally. An estimate of β_{eff} can be found by Bretscher's approximation [5]):

$$\beta_{eff} = \frac{k_{\text{eff}}^{\text{total}} - k_{\text{eff}}^{\text{prompt}}}{k_{\text{eff}}^{\text{total}}} \tag{7}$$

To run a prompt-only eigenvalue calculation with Shift, enable the following parameter in the *SHIFT* block.

Listing 4. Example Shift input to run prompt eigenvalue calculation.

```
[SHIFT][KCODE]
prompt_only true
```

This capability was also integrated into all SCALE sequences that use `Shift` and can be enabled by setting the PNU parameter to "YES" in the parameters block of a SCALE input.

A validation of the prompt eigenvalue implementation was performed using a Molten Salt Reactor Experiment (MSRE) 2D pincell provided by Kyoung Lee [6], as shown in Figure 3. The SCALE model for the prompt calculation is shown in Listing A.1, and the `Shift` input (which uses the SCALE model) is shown in Listing A.2. This problem was run through SCALE using the Criticality Safety Analysis Sequence (CSAS) sequence, utilizing both KENO6 and `Shift` for the MC transport. Table 1 shows the resulting total and prompt eigenvalues, along with estimated and calculated β_{eff}, using CSAS results as the reference. All eigenvalues and estimated β_{eff} are within 2σ, and the tallied β_{eff} = 651 pcm, which also coincides with the estimated values shown in Table 1.

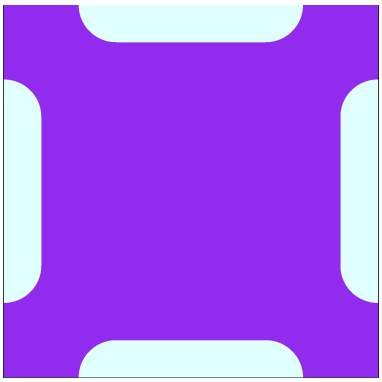

Figure 3. MSRE 2D pincell.

Table 1. MSRE 2D pincell prompt eigenvalue comparison.

Code	k_{eff}^{total}	$\delta k_{\text{eff}}^{total}$ **[pcm]**	k_{eff}^{prompt}	$\delta k_{\text{eff}}^{prompt}$ **[pcm]**	β_{eff} **[pcm]**	$\delta\beta_{\text{eff}}$ **[pcm]**
CSAS	1.63692 ± 0.00005		1.62618 ± 0.00005		656 ± 4	
CSAS-Shift	1.63665 ± 0.00011	28 ± 5	1.62616 ± 0.00012	1 ± 5	641 ± 10	16 ± 11
Shift	1.63671 ± 0.00004	21 ± 5	1.62607 ± 0.00004	11 ± 5	650 ± 4	6 ± 6

2.3 3D ABTR PIN CELL ANALYSIS

Although the focus of this milestone was on PBRs and MSRs, `Shift` can also generate cross sections for fast reactors. An effort was initiated in the summer of 2023 to investigate `Shift` for generating heterogeneous macroscopic cross section sets for fast reactors as an alternative pathway for generating cross sections for `Griffin`. A 3D pincell from the Advanced Breeder Test Reactor (ABTR) benchmark [7] was used as a test problem to analyze MC-generated multigroup cross sections. Inputs for `Shift` and `Serpent` were created to generate 9-group and 33-group homogenized macroscopic cross sections for six material regions corresponding to lower reflector, cladding, sodium coolant, fuel, helium gap, and upper reflector (9-group inputs are shown in Listings B.1, B.2, and B.3). Corresponding `Griffin` transport inputs were created to calculate k_{eff} using these generated homogenized cross sections with P_0, P_1, and P_2 scattering moments (9-group P_0 input shown in Listing B.4).

Figure 4 shows a radial and axial slice of the pincell model. The 9-group and 33-group energy structures are based on ANL bounds and are shown in Tables 2 and 3. Reaction rates and fluxes in `Shift` and `Serpent` were tallied on 90-group and 330-group intermediate energy structures, as shown in Tables B.1, B.2, B.3, and B.4, by splitting each 9-group and 33-group interval into ten equal-lethargy bins.

First, a comparison of the generated homogenized cross sections is shown in Figures 5 and 12. The `Shift` and `Serpent` total, absorption, fission, nu-fission, and transport cross sections agree very well for both 9-group and 33-group structures. The larger differences in the helium gap transport cross section are due to the data modeling differences between these codes.

The 9-group scattering cross section moment comparisons for each homogenized region are shown in Figures 6– 11. The 33-group scattering cross section moment comparisons for each homogenized region are shown in Figures 13– 18. Note that these figures show the logarithm of the ratio of `Serpent` to `Shift` values. Overall, and as expected, `Shift` and `Serpent` results for the 9-group and 33-group P_0 scattering cross sections agree better than those of the higher moments.

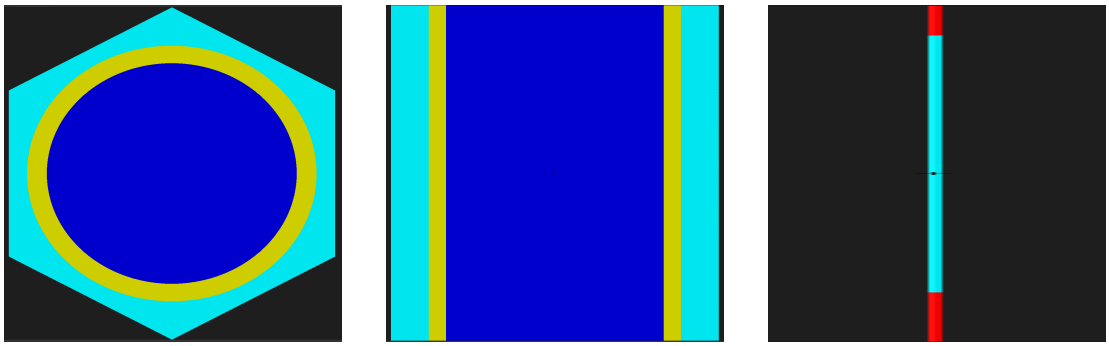

(a) X-Y slice at axial midplane **(b) Y-Z slice at origin** **(c) Full axial slice**

Figure 4. 3D ABTR pincell (fuel = dark blue, clad = yellow, coolant = cyan, reflector = red, helium gap is too small to see).

Second, along with the higher-order scattering moments, TCP_0-corrected scattering cross sections were also calculated and used in `Griffin`. Tables 4 and 5 show the 3D ABTR pincell k_{eff} comparisons between `Shift`, `Serpent`, and `Griffin`. `Shift` and `Serpent` k_{eff} agree within 50 pcm, which gives confidence that the models are consistent. The `Griffin`-calculated k_{eff} shows a similar trend when using increasing scattering moments generated by `Shift` and `Serpent`, with all of these grossly over-predicting k_{eff}. However, the closest eigenvalue to the MC solution was achieved when using the TCP_0-corrected scattering cross section (under-predicting as expected). This result leads to the conclusion that higher-order scattering matrix tallies might need to be weighted by higher-order flux moments instead of the scalar (P_0) flux to produce more accurate scattering moments.

Table 2. Nine (9) coarse-group energy bounds for ABTR pincell homogenized cross sections.

Grp	Upper Energy (eV)	Grp	Upper Energy (eV)
1	1.419×10^7	6	9.119×10^3
2	2.231×10^6	7	2.035×10^3
3	8.208×10^5	8	4.540×10^2
4	1.832×10^5	9	5.043×10^0
5	4.087×10^4		

Table 3. Thirty-three (33) coarse-group energy bounds for ABTR pincell homogenized cross sections.

Grp	Upper Energy (eV)	Grp	Upper Energy (eV)	Grp	Upper Energy (eV)
1	1.419×10^7	12	6.738×10^4	23	2.754×10^2
2	1.000×10^7	13	4.087×10^4	24	1.670×10^2
3	6.065×10^6	14	2.479×10^4	25	1.013×10^2
4	3.679×10^6	15	1.503×10^4	26	6.144×10^1
5	2.231×10^6	16	9.119×10^3	27	3.727×10^1
6	1.353×10^6	17	5.531×10^3	28	2.260×10^1
7	8.209×10^5	18	3.355×10^3	29	1.371×10^1
8	4.979×10^5	19	2.035×10^3	30	8.315×10^0
9	3.020×10^5	20	1.234×10^3	31	3.928×10^0
10	1.832×10^5	21	7.485×10^2	32	5.316×10^{-1}
11	1.111×10^5	22	4.540×10^2	33	4.175×10^{-1}

Table 4. Nine (9)-group ABTR k_{eff} Comparison.

Code	k_{eff}	δk_{eff} [pcm])
Shift	1.43546	
Serpent	1.43592	46
Shift-Griffin P_0	1.46605	3059
Shift-Griffin P_1	1.44241	695
Shift-Griffin P_2	1.44268	722
Shift-Griffin TCP_0	1.43761	215
Serpent-Griffin P_0	1.46646	3054
Serpent-Griffin P_1	1.44275	683
Serpent-Griffin P_2	1.44303	711
Serpent-Griffin TCP_0	1.43795	203

Table 5. Thirty-three (33)-group ABTR k_{eff} Comparison.

Code	k_{eff}	δk_{eff} [pcm]
Shift	1.43546	
Serpent	1.43592	46
Shift-Griffin P_0	1.46596	3050
Shift-Griffin P_1	1.44135	589
Shift-Griffin P_2	1.44165	619
Shift-Griffin TCP_0	1.43464	-82
Serpent-Griffin P_0	1.46642	3050
Serpent-Griffin P_1	1.44174	582
Serpent-Griffin P_2	1.46165	2573
Serpent-Griffin TCP_0	1.43500	-92

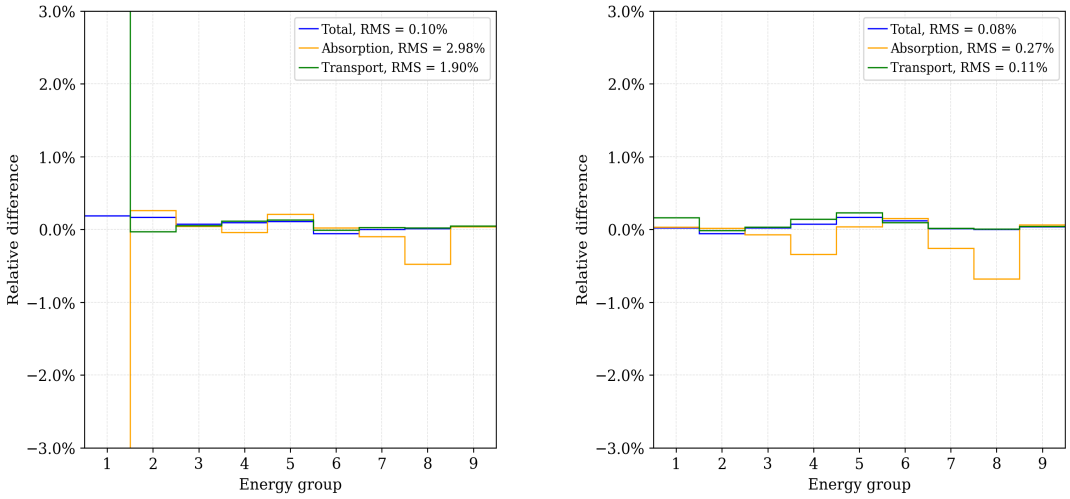

(a) Lower reflector

(b) Clad

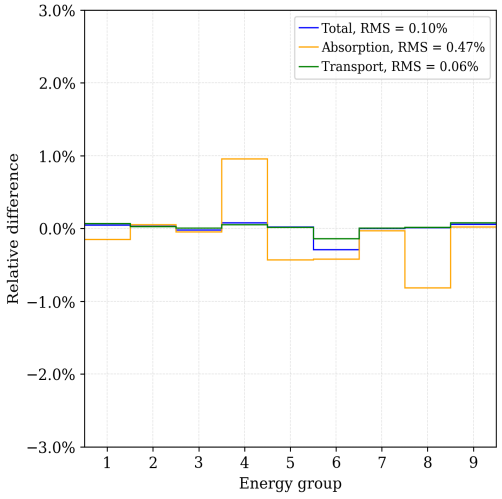

(c) Coolant

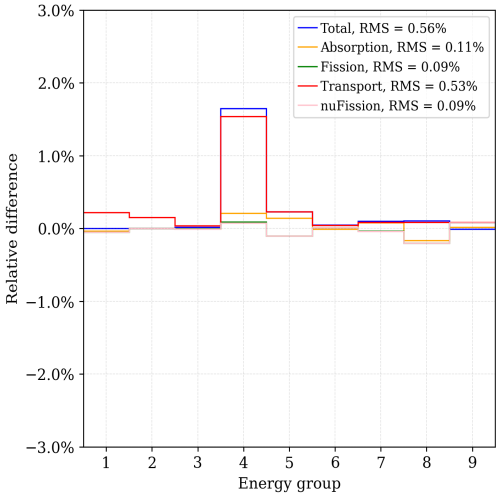

(d) Fuel

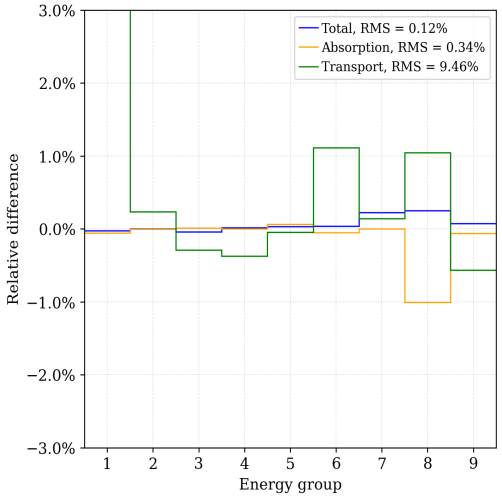

(e) Helium gap

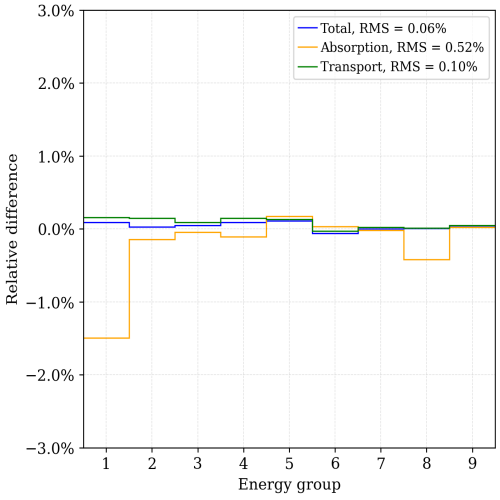

(f) Upper reflector

Figure 5. Three-dimensional ABTR pincell 9-group cross section comparison.

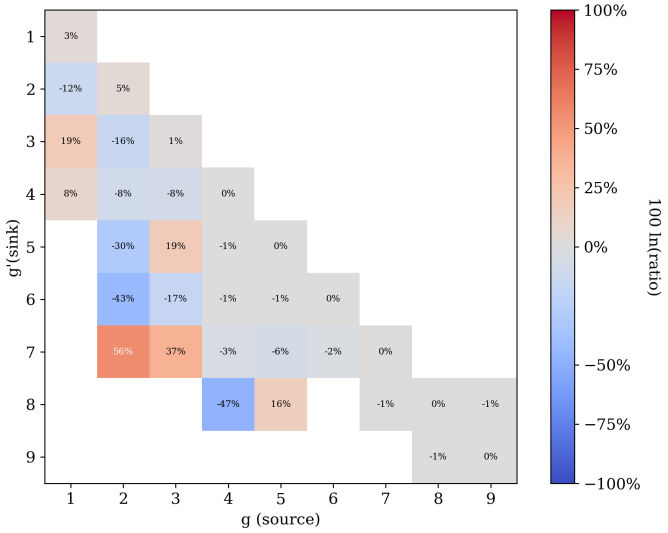

(a) P_0

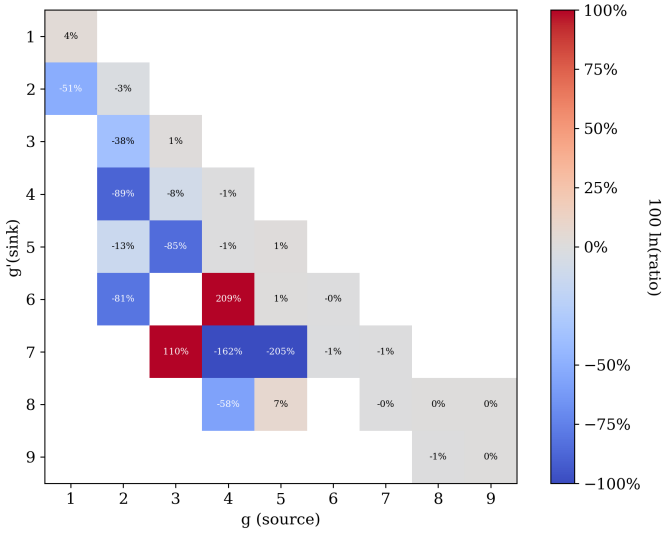

(b) P_1

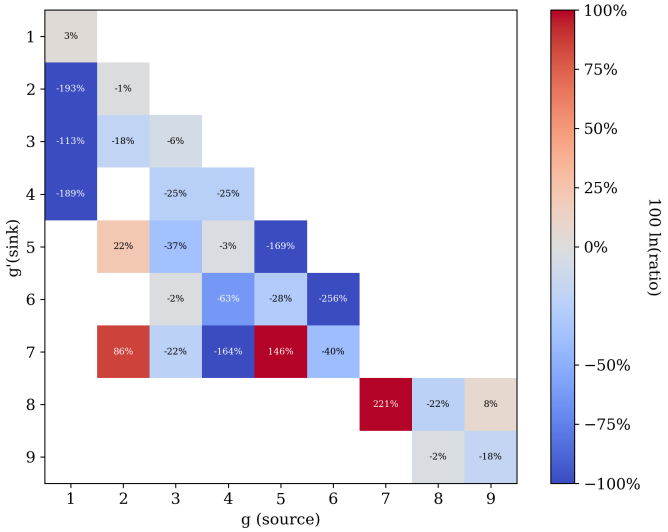

(c) P_2

Figure 6. Three-dimensional ABTR pincell 9-group lower reflector scattering cross section moments comparison.

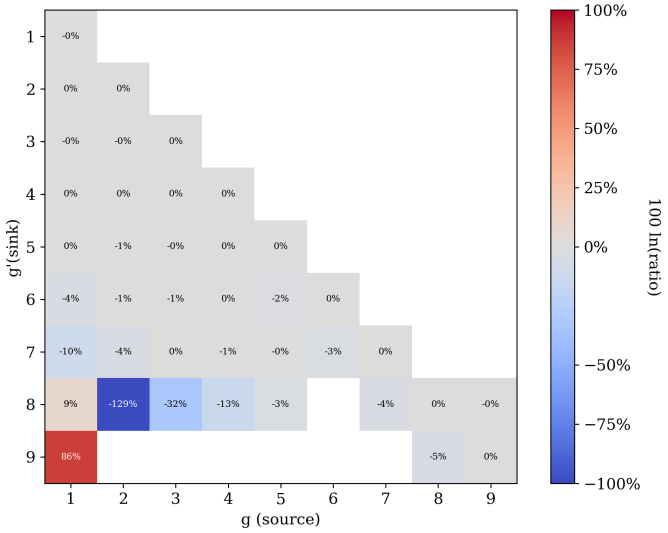

(a) P_0

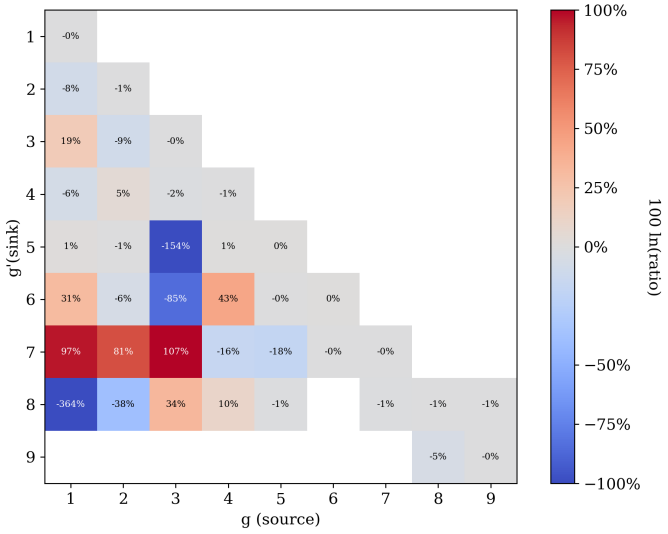

(b) P_1

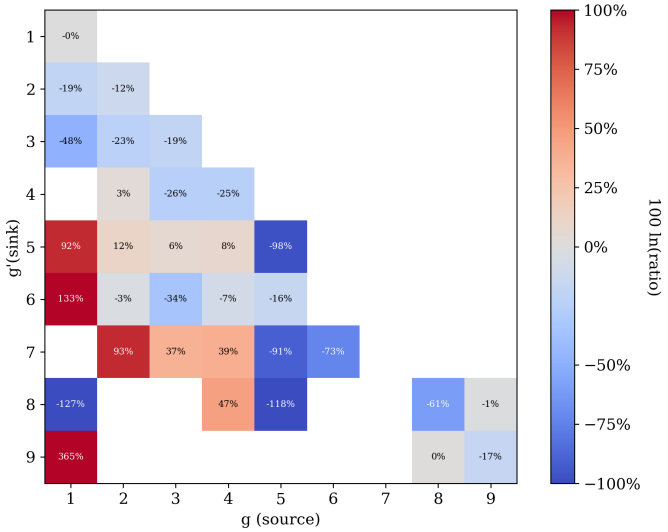

(c) P_2

Figure 7. Three-dimensional ABTR pincell 9-group clad scattering cross section moments comparison.

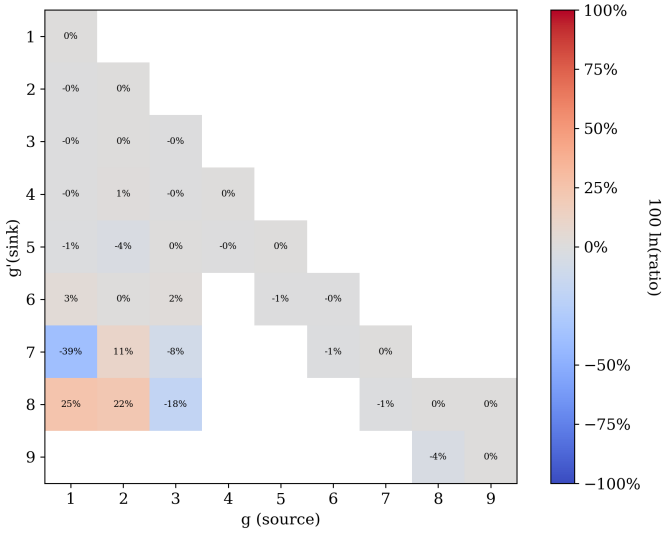

(a) P_0

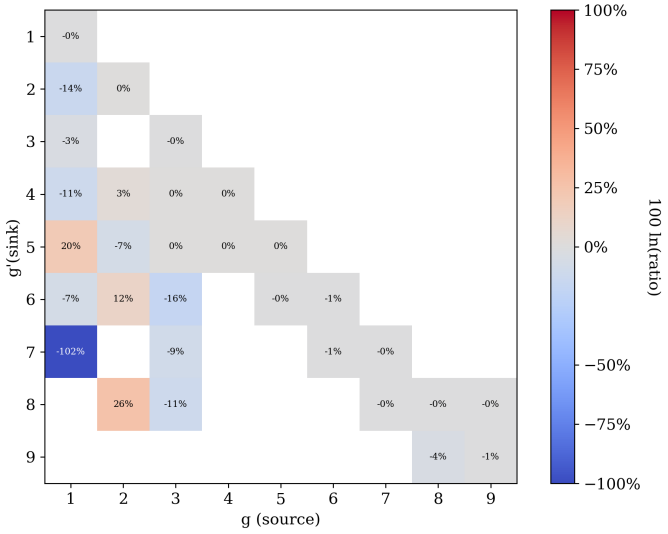

(b) P_1

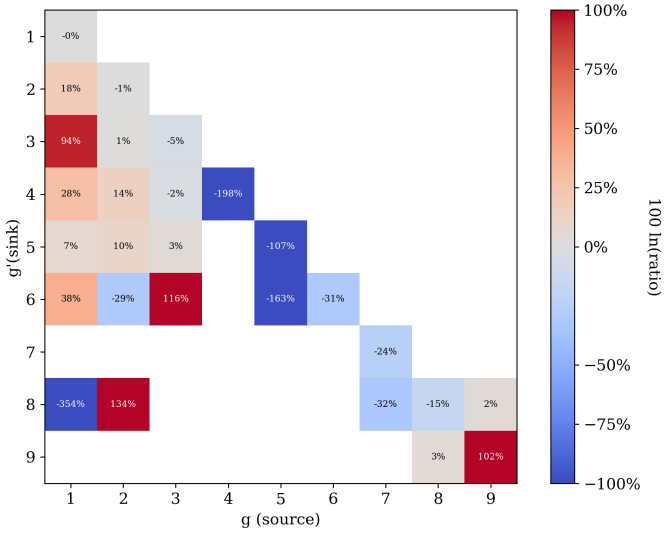

(c) P_2

Figure 8. Three-dimensional ABTR pincell 9-group coolant scattering cross section moments comparison.

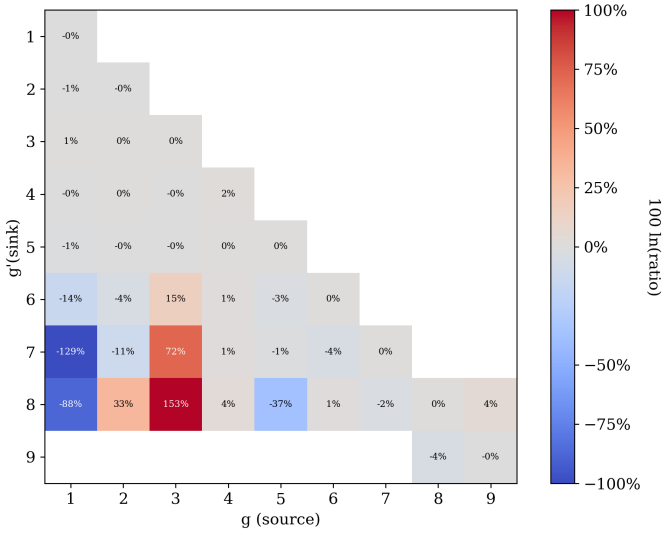

(a) P_0

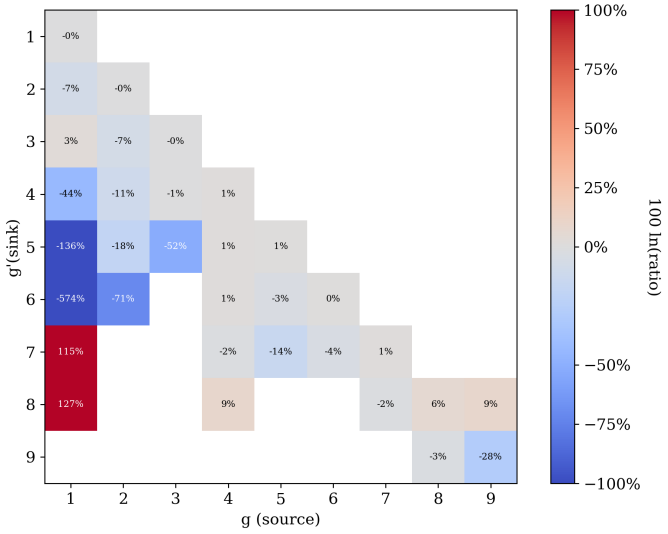

(b) P_1

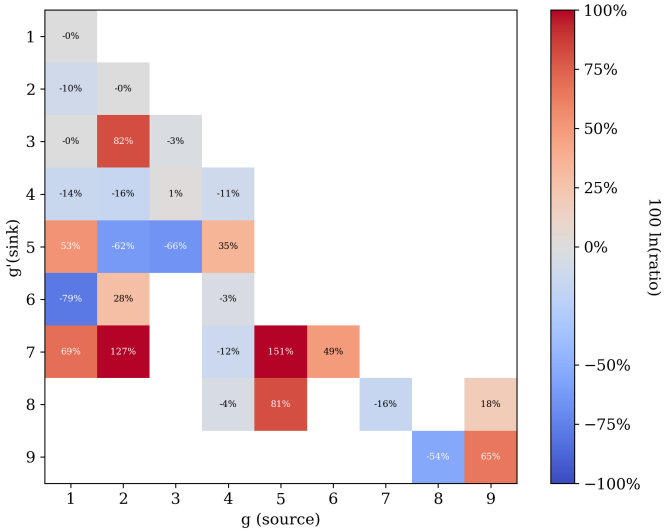

(c) P_2

Figure 9. Three-dimensional ABTR pincell 9-group fuel scattering cross section moments comparison.

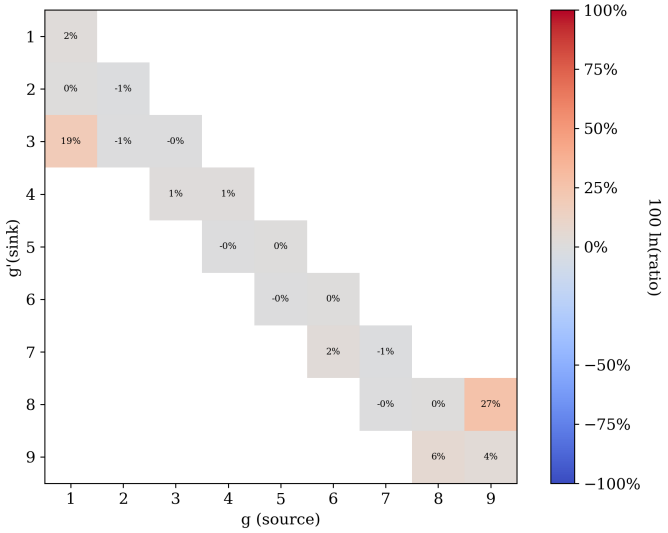

(a) P_0

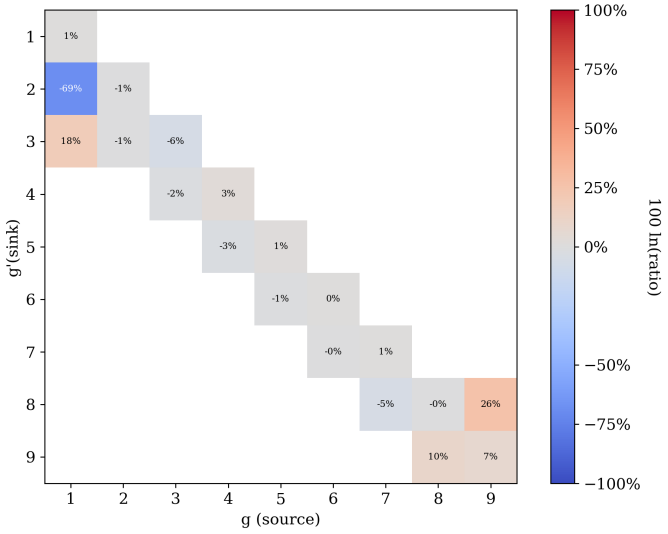

(b) P_1

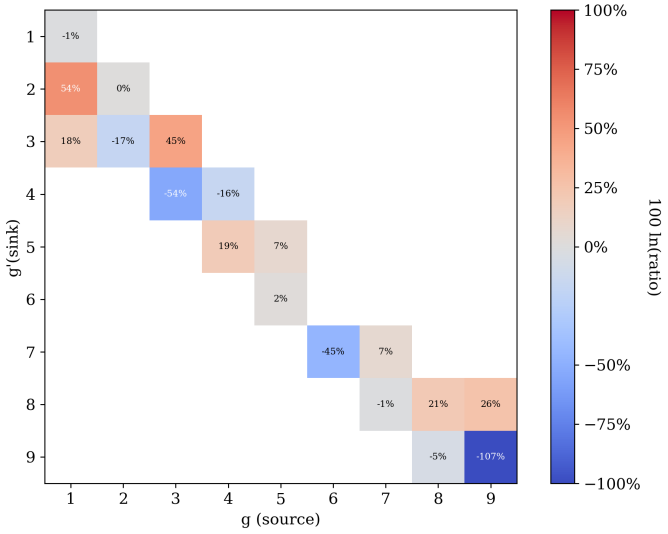

(c) P_2

Figure 10. Three-dimensional ABTR pincell 9-group gap scattering cross section moments comparison.

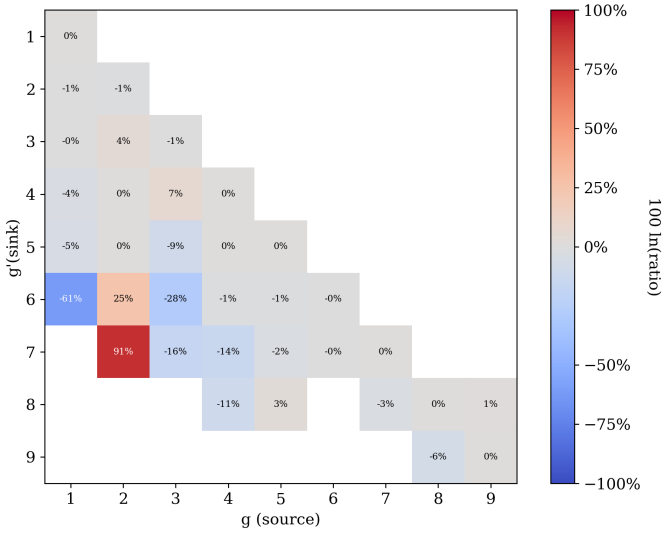

(a) P_0

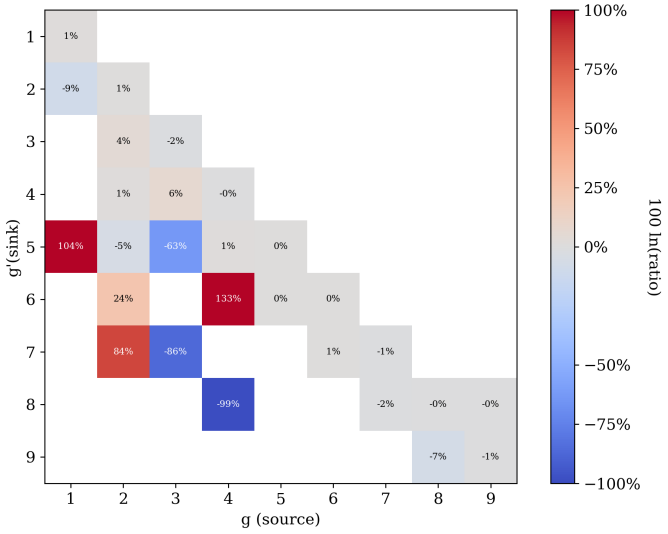

(b) P_1

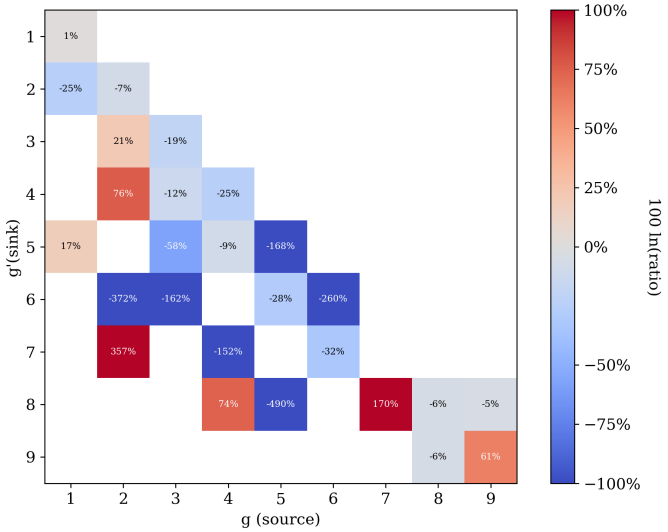

(c) P_2

Figure 11. Three-dimensional ABTR pincell 9-group upper reflector scattering cross section moments comparison.

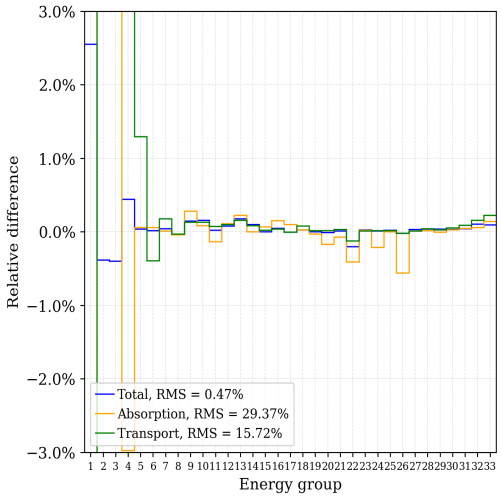

(a) Lower reflector

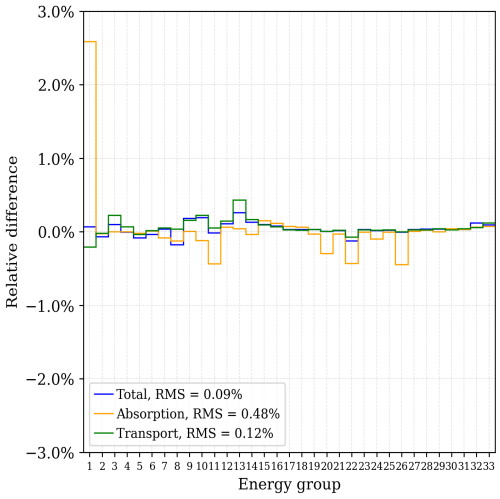

(b) Clad

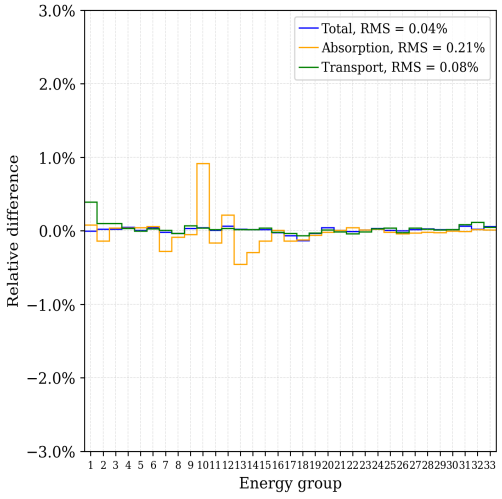

(c) Coolant

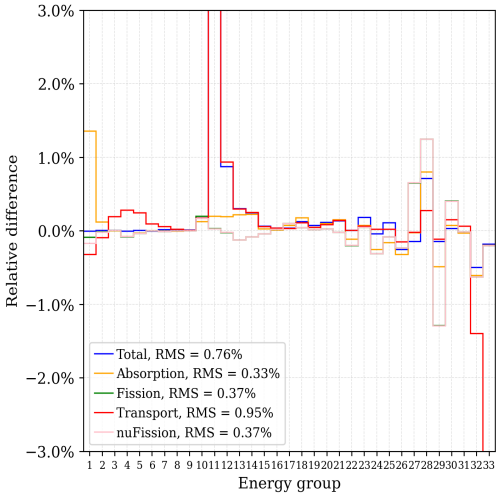

(d) Fuel

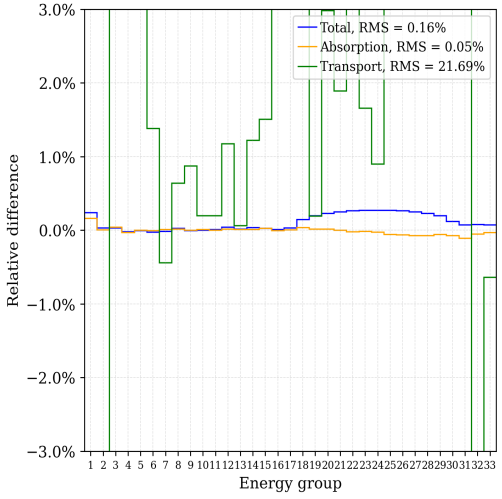

(e) Helium gap

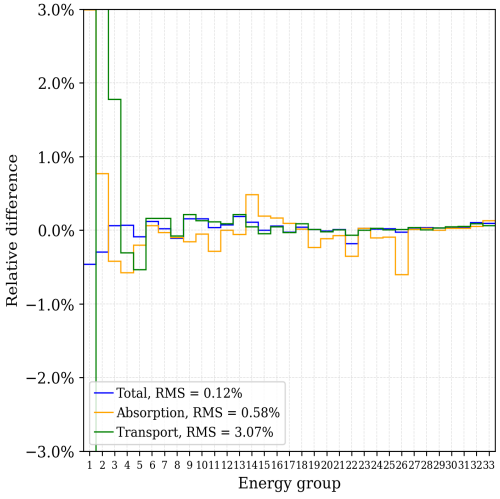

(f) Upper reflector

Figure 12. Three-dimensional ABTR pincell 33-group cross section comparison.

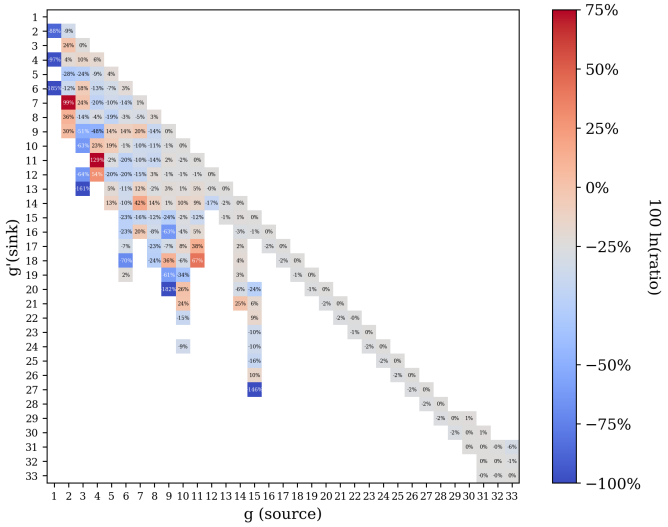

(a) P_0

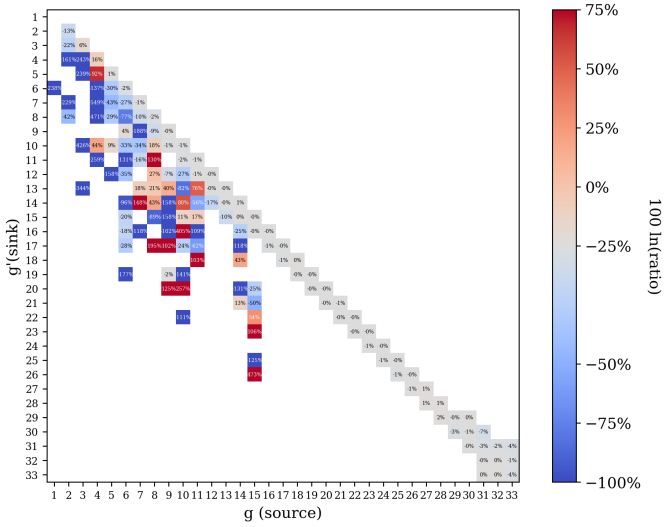

(b) P_1

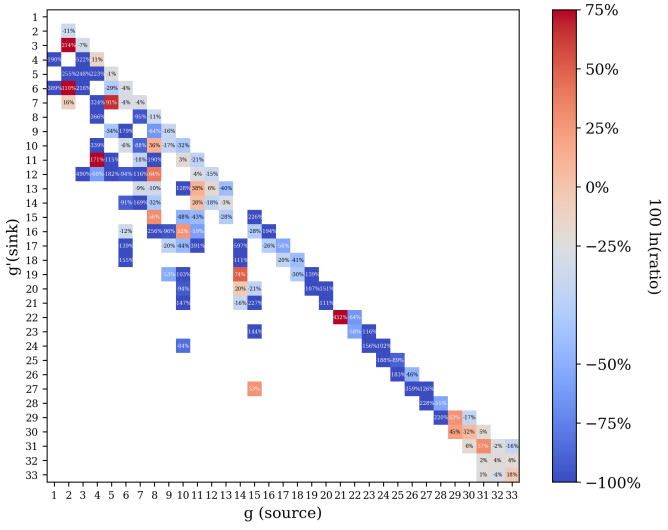

(c) P_2

Figure 13. Three-dimensional ABTR pincell 33-group lower reflector scattering cross section moments comparison.

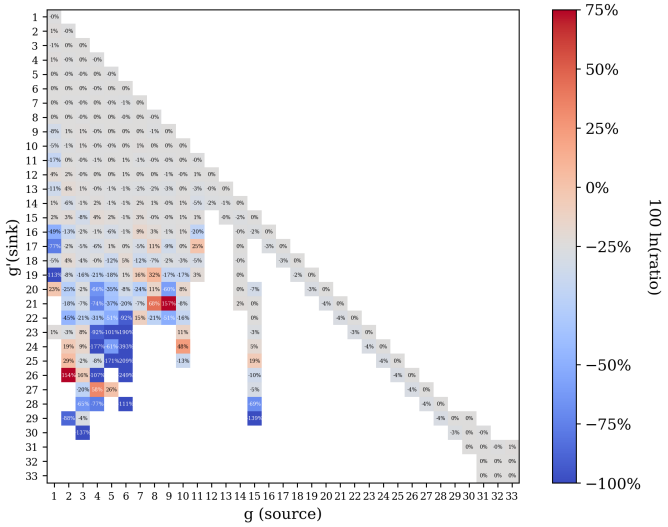

(a) P_0

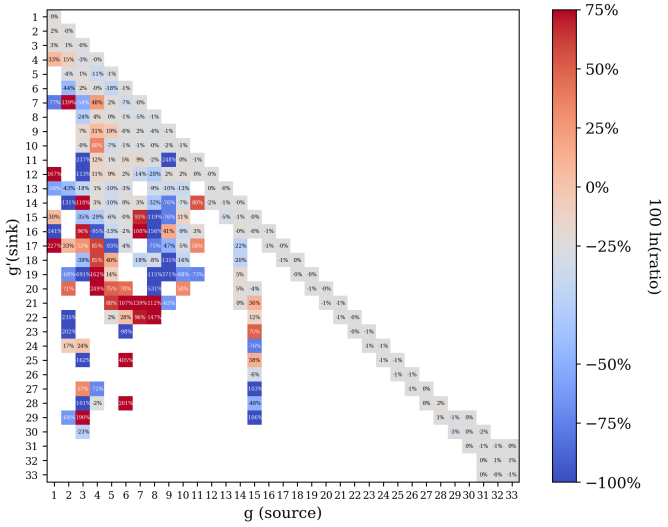

(b) P_1

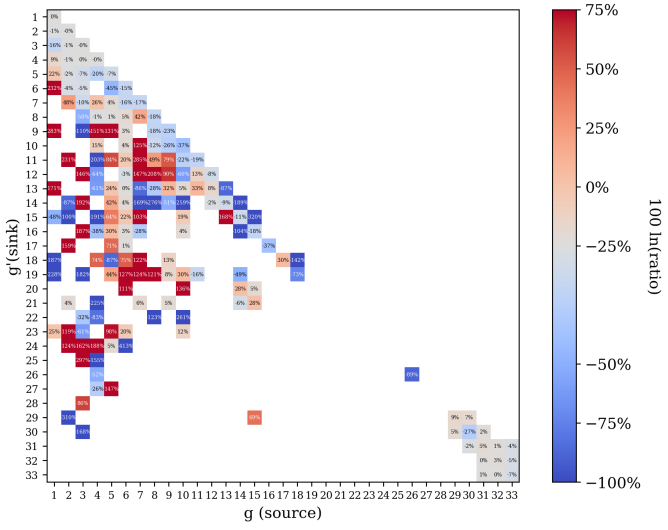

(c) P_2

Figure 14. Three-dimensional ABTR pincell 33-group clad scattering cross section moments comparison.

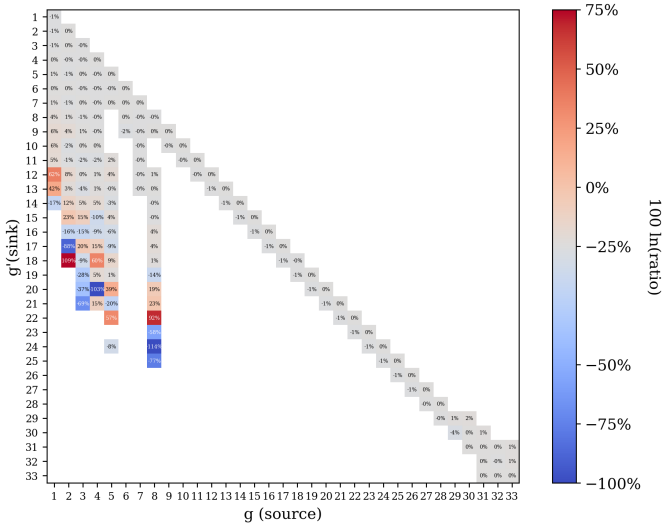

(a) P_0

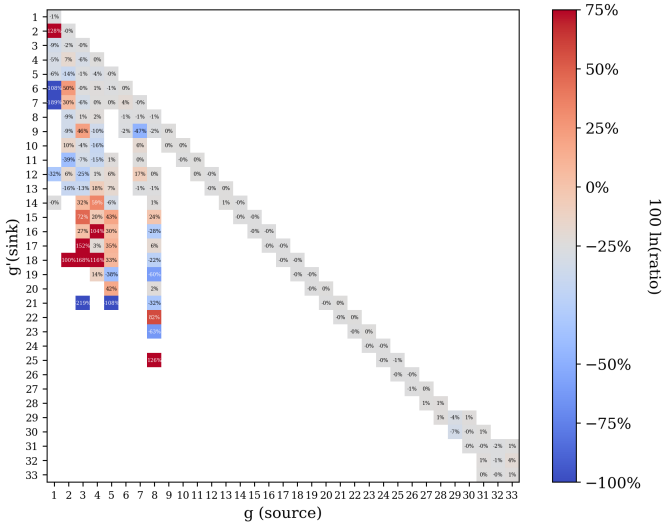

(b) P_1

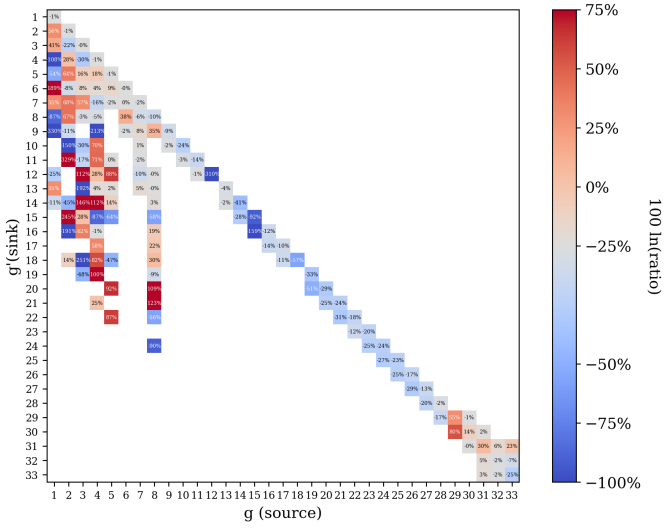

(c) P_2

Figure 15. Three-dimensional ABTR pincell 33-group coolant scattering cross section moments comparison.

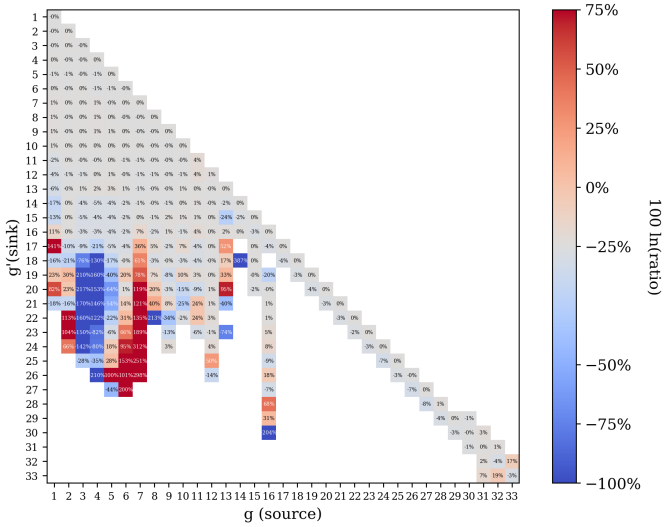

(a) P_0

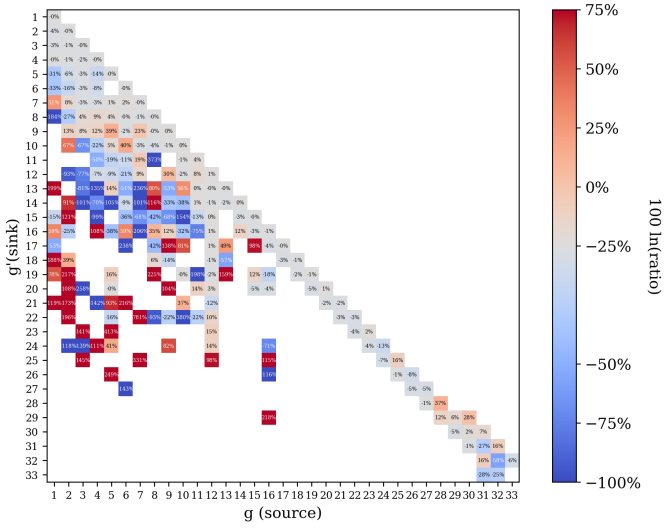

(b) P_1

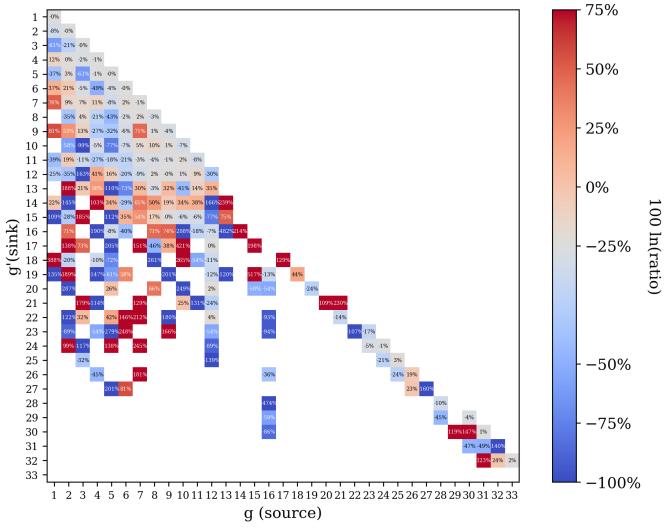

(c) P_2

Figure 16. Three-dimensional ABTR pincell 33-group fuel scattering cross section moments comparison.

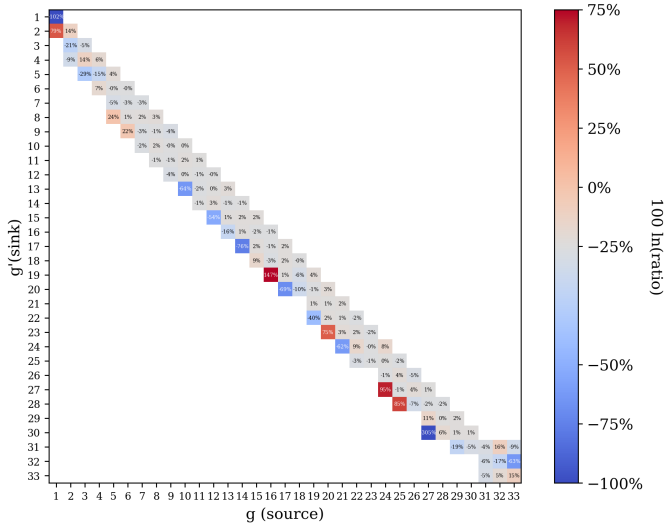

(a) P_0

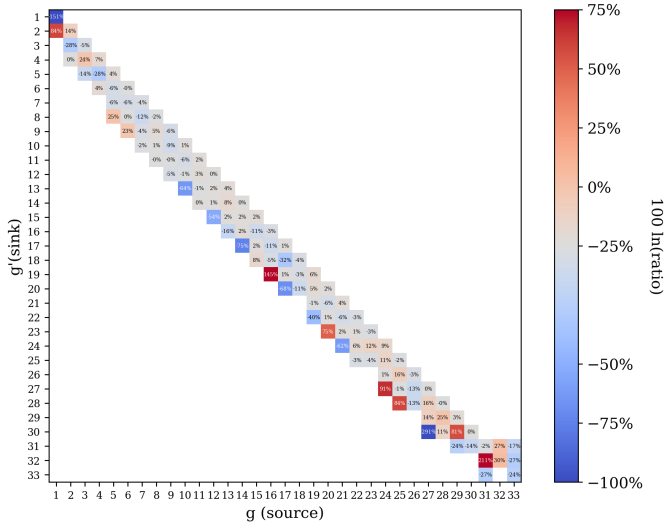

(b) P_1

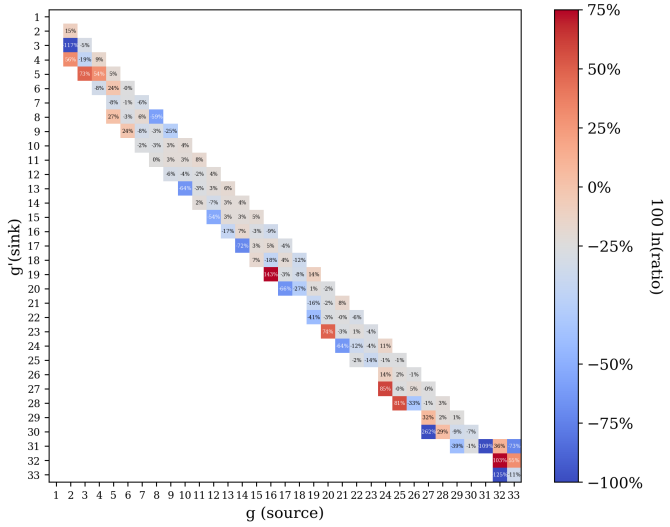

(c) P_2

Figure 17. Three-dimensional ABTR pincell 33-group gap scattering cross section moments comparison.

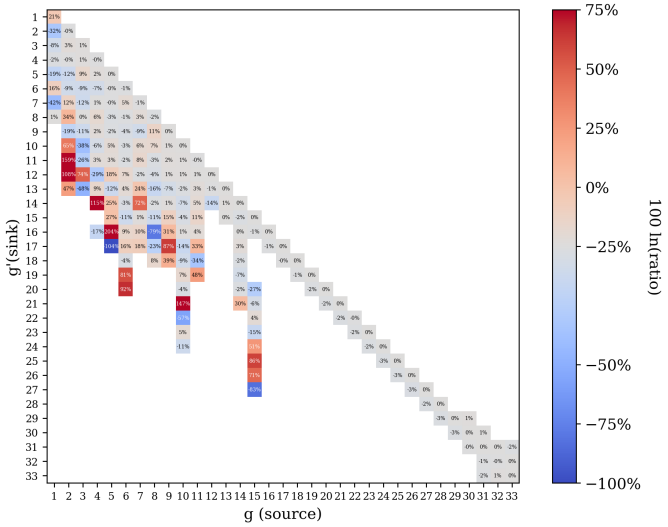

(a) P_0

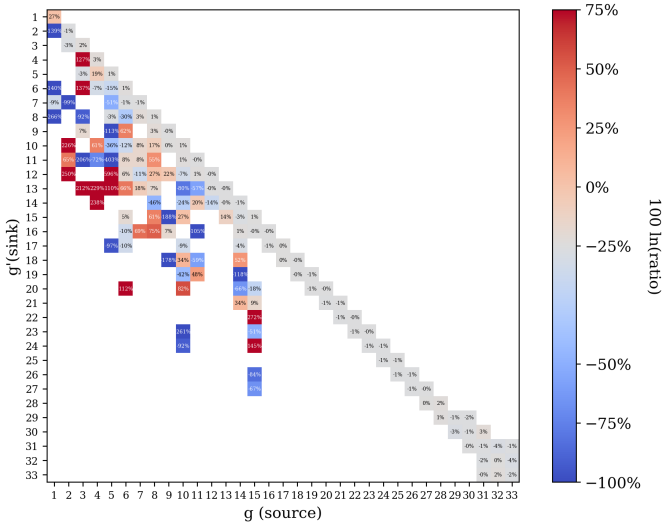

(b) P_1

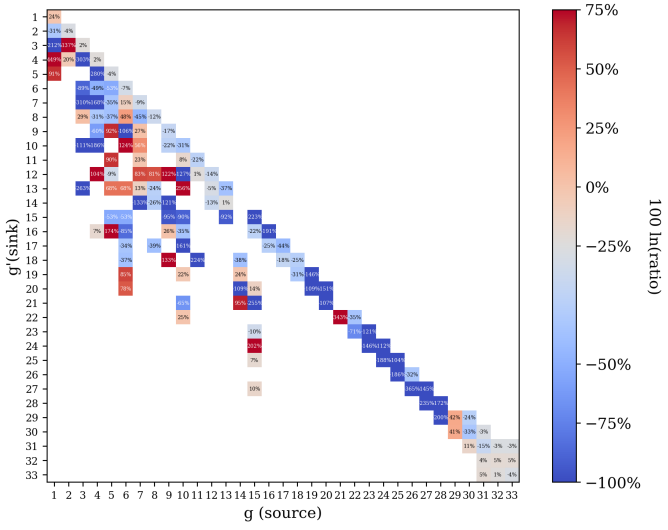

(c) P_2

Figure 18. Three-dimensional ABTR pincell 33-group upper reflector scattering cross section moments comparison.

2.4 FUTURE WORK

To build upon the current multigroup cross section generation capabilities in `Shift`, several features are needed to properly generate the required data for advanced reactor analysis.

- As mentioned above, `Shift` needs to properly tally and calculate the delayed neutron spectrum. Three approaches could be used to calculate the delayed spectrum in `Shift`: First, modify the currently implemented birth spectrum tally to tally the total and prompt production rates. Second, perform partial macroscopic production tallies combined with the multigroup χ distribution from a loaded multigroup library. Third, update the particle information to determine whether it came from a prompt or delayed fission, and then update the birth spectrum tally to properly bin the particle upon its birth.
- Based upon the ABTR analysis, more accurate higher-order scattering matrices can be calculated if flux moment weighting is used instead of weighting only by the zeroth moment (scalar flux). This update will be made to the `Shift` *CELLNODAL* scattering matrix tally.
- As needed for transient (including depletion) deterministic calculations, the ability to calculate and output microscopic cross sections will be added to `Shift`. Efficiently producing accurate microscopic scattering matrices (including those of higher orders) will be the main area of investigation.
- Allow scaling of scalar flux and relevant cross sections (such as κ_{fission}) by a user-input power level with output to HDF5 and ISOXML files. Currently, only the flux can be normalized to a user-provided power level when converting the HDF5 output values to ISOXML.
- Add the ability to tally and produce adjoint-weighted kinetics parameters, which should be more accurate than the currently implemented forward-weighted parameters.

3. TITAN ENHANCEMENTS

The production release of Titan occurred in SCALE7.0b3 (10/1/22). Titan provides an easy-to-use interface for Shift, as well as an application programming interface (API) to build Oak Ridge Adaptable Nested Geometry Engine (ORANGE) geometries for uses such as ray tracing. It can run Shift by reading an input file or by populating a model via an internal API. Titan uses a JSON-formatted input split into three main sections: geometry, materials, and Shift options. The input is validated prior to running Shift.

In FY23, support for many concrete unit types, cell tallies, and high packing fractions for sphere-packed pebbles was added to Titan.

3.1 NEW TITAN UNITS

The supported units added to Titan follow, and example inputs and graphical outputs for each of these outputs are indicated in the figures below.

- **Circle and Extruded Circle Domains**: Figure 19 shows the geometry input and XY graphical output of a Circle Domain with a Polygon Domain inserted.
- **Axial Stack**: Figure 20 shows the geometry input and XY graphical output of an Axial Stack composed of three Extruded Pins.
- **Concentric Sphere**: Figure 21 shows the geometry input and XY graphical output of a Concentric Sphere.
- **Square and Extruded Square Maps**: Figure 22 shows the geometry input and XY graphical output of a Square Map. This Square Map has two Pin elements: a Polygon Domain element and an empty element. The Polygon Domain is offset by an XY translation, and the entire map is rotated 30 degrees.
- **Hex and Extruded Hex Maps**: Figure 23 shows the geometry input and XY graphical output of the Empire 2D assembly, utilizing the Hex Map in Titan.
- **Extruded Pin**: See Fig. 20.
- **Extruded Polygon Domain**: No specific example provided.
- **Pebble**: Figure 24 shows the geometry input and XY graphical output of the HTR-10 fuel pebble, utilizing the Pebble in Titan.

```
"geometry" : {
  "units" : {
    "F" : [ "POLYGON_DOMAIN",
      [
        "FUEL", [6, 0.3,
        {
          "corner_rad" : 0.03,
          "indent_length" : 0.1,
          "indent_thickness" : -0.1
        }]
      ]
    ],
    "W" : [ "CIRCLE_DOMAIN",
      [ "WATER", 0.63,
      {
          "inserts" : [ ["F"] ]
      }]
    ]
  }
}
```

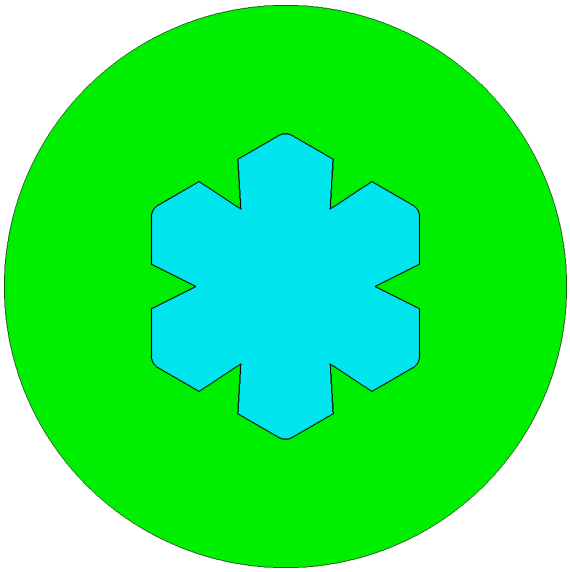

Figure 19. The XY slice of a Circle Domain with a Polygon Domain inserted and its input.

```
"geometry" : {
  "units" : {
      "L" : [ "PIN",
              [ ["WATER", 0.475] ]
      ],
      "M" : [ "PIN",
              [ ["FUEL", 0.4096],
                ["GAP", 0.418],
                ["CLAD",0.475] ]
      ],
      "U" : [ "PIN",
              [ ["GAP", 0.475] ]
      ],
      "STACK" : [ "AXIAL_STACK",
            [ ["L", 0.1],
              ["M", 0.5],
              ["U", 0.1] ]
      ]
  }
}
```

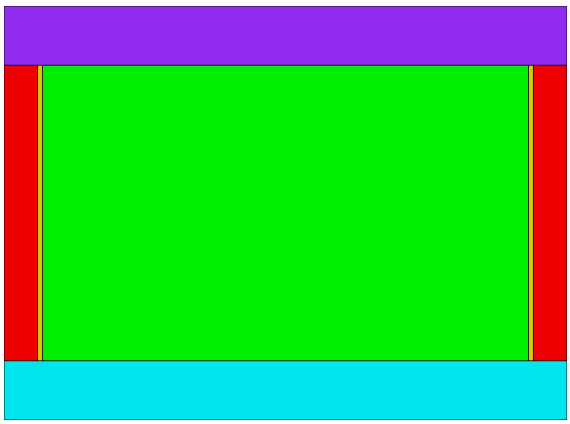

Figure 20. XZ slice of an Axial Stack composed of three Extruded Pins and its input.

```
"geometry" : {
  "units" : {
      "godiva" : [ "CONCENTRIC_SPHERE",
             [ ["FUEL", 8.7407],
               ["GAP", 20.0] ]
      ]
  }
}
```

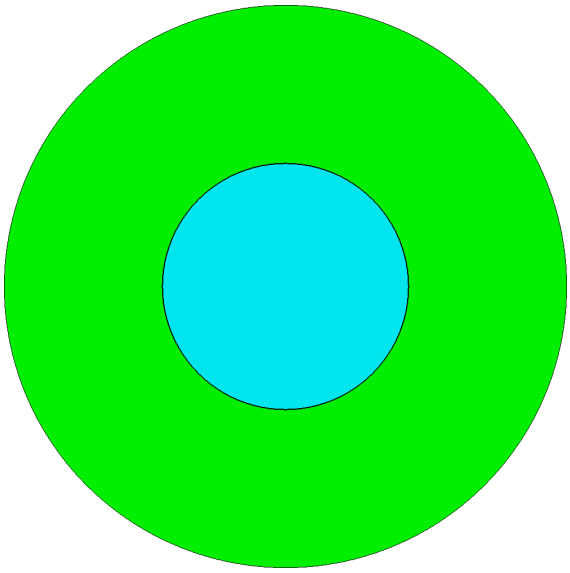

Figure 21. XY slice of a Concentric Sphere and its input.

```
"geometry" : {
  "units" : {
    "F" : ["PIN",
        [ ["FUEL", 0.4096],
          ["GAP", 0.418],
          ["CLAD",0.475] ]
    ],
    "G" : ["POLYGON_DOMAIN",
        ["GAP", [4, 0.475] ]
    ],
    "MAP" : ["SQUARE_MAP",
        {
            "dim" : 2,
            "pitch" : 1.26,
            "fill" : "WATER",
            "rotation" : 30.0,
            "elements" : [
                ["F", "G"],
                ["-", "F"]
            ],
            "offsets" : [
                [0,1,[["TRANSLATE_XY",[0.1,-0.05]]]]
            ],
            "rotation" : 30.0
        }
    ]
  }
}
```

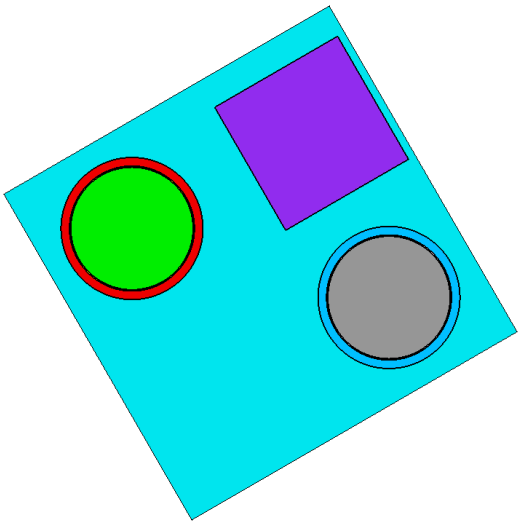

Figure 22. XY slice of an example Square Map and its input.

```
"geometry" : {
  "units" : {
    "F" : [ "PIN",
        [ [ "FUEL", 0.925 ],
          [ "GAP",  0.975  ] ]
    ],
    "H" : [ "PIN",
        [ [ "COOL", 1.0 ] ]
    ],
    "M" : [ "PIN",
        [ [ "MOD", 0.95 ],
          [ "GAP",  1.0  ] ]
    ],
    "ASSM" : [ "HEX_MAP",
        {
        "pitch" : 1.075,
        "fill" : "STRUCT",
        "map_apothem" : 16.13695,
        "rotation" : 0.0,
        "num_rings" : 9,
        "elements" : [
                          [ "H", "F", "H", "F", "H", "F", "H", "F", "H" ],
                        [ "F", "M", "M", "M", "M", "M", "M", "M", "M", "F" ],
                      [ "H", "M", "H", "F", "H", "F", "H", "F", "H", "M", "H" ],
                    [ "F", "M", "F", "M", "M", "M", "M", "M", "M", "F", "M", "F" ],
                  [ "H", "M", "H", "M", "H", "F", "H", "F", "H", "M", "H", "M", "H" ],
                [ "F", "M", "F", "M", "F", "M", "M", "M", "M", "F", "M", "F", "M", "F" ],
              [ "H", "M", "H", "M", "H", "M", "H", "F", "H", "M", "H", "M", "H", "M", "H" ],
            [ "F", "M", "F", "M", "F", "M", "F", "M", "M", "F", "M", "F", "M", "F", "M", "F" ],
          [ "H", "M", "H", "M", "H", "M", "H", "M", "H", "M", "H", "M", "H", "M", "H", "M", "H" ],
            [ "F", "M", "F", "M", "F", "M", "F", "M", "M", "F", "M", "F", "M", "F", "M", "F" ],
              [ "H", "M", "H", "M", "H", "M", "H", "F", "H", "M", "H", "M", "H", "M", "H" ],
                [ "F", "M", "F", "M", "F", "M", "M", "M", "M", "F", "M", "F", "M", "F" ],
                  [ "H", "M", "H", "M", "H", "F", "H", "F", "H", "M", "H", "M", "H" ],
                    [ "F", "M", "M", "M", "M", "M", "M", "M", "M", "F" ],
                      [ "H", "F", "H", "F", "H", "F", "H", "F", "H" ]
      ]
    }],
    "EMPIRE_ASSEMBLY": ["POLYGON_DOMAIN",
        ["GAP", [6, 16.75, {"rotation": 30.0}],
        {
         "inserts" :[ ["ASSM"] ]
        }]
    ]
  }
```

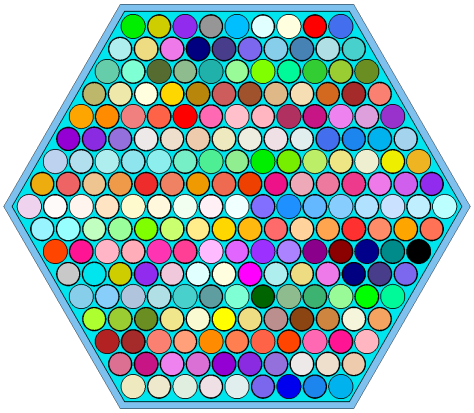

Figure 23. XY slice of the Empire 2D assembly and its input.

```
"geometry" : {
  "units" : {
      "TRISO" : [ "CONCENTRIC_SPHERE",
                  [["FUEL", 0.0250],
                  ["BUFFER", 0.0340],
                  ["IPC", 0.0380],
                  ["SiC", 0.0415],
                  ["OPC", 0.0455]]
      ],
      "F" : [ "PEBBLE",
        {
          "pebble" : [
              ["MATRIX", 2.5],
              ["SHELL",3.0]
           ],
           "particle" : "TRISO",
           "num_particles" : 8385,
           "accel_grid_density": 2.0
        }
      ]
  }
}
```

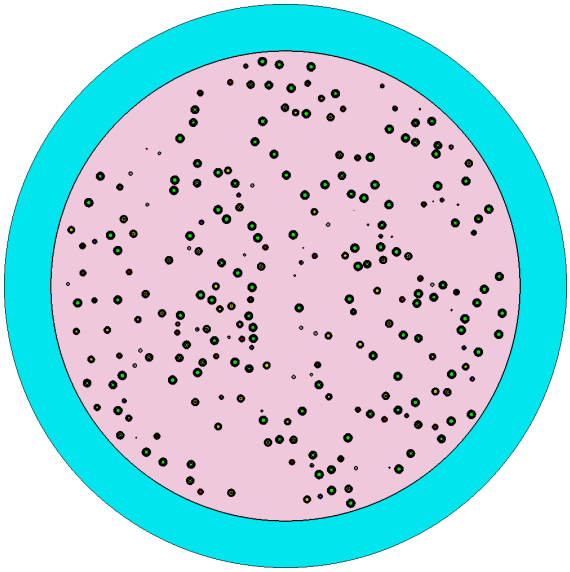

Figure 24. XY slice of the HTR-10 fuel pebble and its input.

3.2 CELL TALLIES

`Titan` allows for energy-dependent and energy-integrated cell union tallies on specific reaction types and any supported ENDF MT number. Table 6 contains the currently supported reaction types (beyond all ENDF MT values) in `Titan`.

Table 6. Supported cell tally reaction types in Titan.

total	fission
flux	kappa_sigma_f
nu_fission	kappa_sigma_c
nu_delayed_fission	chi
scattering	pos_partial_current_x
transfer_1n	neg_partial_current_x
transfer_2n	pos_partial_current_y
transfer_3n	neg_partial_current_y
transfer_4n	pos_partial_current_z
absorption	neg_partial_current_z

To verify the `Titan` cell tally capability, a pincell was run through the `Titan` and `Omnibus` frontends. Listing 5 shows a partial input of a pincell in `Titan` with two cell tallies defined: `Fuel Pin Tally` and `Energy Pin Tally`. The `Fuel Pin Tally` is an energy-integrated absorption tally over all cells in units `F` and `W`. The `Fuel Energy Tally` is an energy-dependent flux tally over just the `FUEL` region in unit `F`. Its energy boundaries are the user-defined `fast` energy boundaries.

Listing 6 shows the JSON-formatted tally output. The `keff` tally values are output by default, followed by multi-group cell tally results for every user-defined tally. Table 7 and Table 8 show a comparison of the `Titan` and `Omnibus` result. The small differences seen are expected due to the default fission source setup difference.

Listing 5. Titan pincell example input with two different cell tallies.

```
{
  "geometry" : {
    "units" : {
        "F" : [ "PIN",
                [ ["FUEL", 0.4096],
                  ["GAP", 0.418],
                  ["CLAD",0.475] ]
        ],
        "W" : [ "POLYGON_DOMAIN",
           ["WATER", [4, 0.63],
           {
             "inserts" : [ ["F"] ]
           }]
        ]
    }
  },
  "energy_bounds" : {
      "fast" : ["USER", [14.0E+07, 10.0, 1.0E-05] ]
  },
  "tallies" : {
      "Fuel Pin Tally" : [ "CELL", {
          "unit_tallies" : [
              ["F"],
              ["W"]
          ],
          "reactions" : ["absorption"]
      }],
      "Fuel Energy Tally" : [ "CELL" , {
          "unit_tallies" : [
              ["F", {"materials" : ["FUEL"]} ]
          ],
          "bounds" : "fast"
      }]
  }
}
```

Listing 6. Titan pincell example tally output.

```
{
    "keff": {
        "mean": 1.56280141923603,
        "sdev": 0.0008237659950255459
    },
    "mg_tally_results": {
        "Fuel Energy Tally": {
            "bounds": "fast",
            "cell_tally_results": [
                {
                    "mg": [
                        {
                            "mean": 2.139980654873028,
                            "sdev": 0.001115308452725335
                        },
                        {
                            "mean": 0.11135957157741452,
                            "sdev": 0.0001845244887211092 2
                        }
                    ],
                    "name": "[FUEL]cell[1] flux",
                    "total": {
                        "mean": 2.251340226450464,
                        "sdev": 0.001119490327018
                    },
                    "volume": 5.270717853328914
                }
            ]
        },
        "Fuel Pin Tally": {
            "bounds": "-",
            "cell_tally_results": [
                {
                    "mg": [],
                    "name": "[FUEL]cell[1] absorption",
                    "total": {
                        "mean": 0.06919164041510173,
                        "sdev": 6.174595996437717e-05
                    },
                    "volume": 5.270717853328914
                },
                {
                    "mg": [],
                    "name": "[GAP]cell[2] absorption",
```

```
                    "total": {
                        "mean": 1.8180606231632747e-11,
                        "sdev": 2.3433503794028157e-14
                    },
                    "volume": 0.21839849472931572
                },
                {
                    "mg": [],
                    "name": "[CLAD]cell[3] absorption",
                    "total": {
                        "mean": 0.00047202042706669437,
                        "sdev": 3.06685732173681e-06
                    },
                    "volume": 1.5991020766037405
                },
                {
                    "mg": [],
                    "name": "unit[1](POLYGON_DOMAIN).bg absorption",
                    "total": {
                        "mean": 0.0007427047250423921,
                        "sdev": 1.2542034227309855e-06
                    },
                    "volume": 8.787781575338027
                },
                {
                    "mg": [],
                    "name": "cell_union absorption",
                    "total": {
                        "mean": 0.023429777663437547,
                        "sdev": 2.057332126270499e-05
                    },
                    "volume": 15.875999999999998
                }
            ]
        }
    }
}
```


Table 7. Omnibus and Titan pincell example results for the Fuel Pin Tally.

Fuel Pin Tally (rxn/cm^3-particle)			
Tally Name	**Omnibus**	**Titan**	**Rel. Diff.**
[FUEL]cell[1] absorption	0.068958(61)	0.069192(62)	0.35%
[GAP]cell[2] absorption	1.8259(24)e-11	1.8180(23)e-11	0.43%
[CLAD]cell[3] absorption	0.0004610(29)	0.0004720(31)	2.4%
unit1.bg absorption	0.0007522 (13)	0.0007427(13)	1.4%
cell_union absorption	0.023356(20)	0.023430(21)	0.31%

Table 8. Omnibus and Titan pincell example results for the Fuel Energy Tally.

Fuel Energy Tally (rxn/cm^3-particle)				
Tally Name	**Energy Group**	**Omnibus**	**Titan**	**Rel. Diff.**
[FUEL]cell[1] flux	1	2.1415(11)	2.1378(11)	0.17%
	2	0.11065(18)	0.11154(18)	0.80%
	total	2.2522(11)	2.2494(11)	0.12%

3.3 SPHERE-PACKING PROGRESS

Inspired by previous sphere-packing work done by Lozano et al. [8], `Titan` implemented a version of this packing generation algorithm to achieve packing fractions greater than 50% in a spherical domain (Fig. 25).

Algorithm 1 walks through the high-level process of generating close-packed spheres of multiple sizes in a spherical domain. For details on generating the candidate point list for new sphere placement, see details in Sections 3.3 and 3.4 of Lozano's journal article [8].

Algorithm 1: Titan's high packing fraction sphere-packing algorithm.

```
Given     : Desired number of particles of each particle type = count
Given     : Radii of each particle type = radii
// Mesh accelerates neighbor detection
Generate: Cartesian mesh of bounding sphere with mesh cell size based on largest particle radius
Generate: 3 seed spheres tangent to each other and add to queue
/* While spheres are still in the queue and there are still particles to
   place                                                                  */
while !queue.empty() and count > 0 do
    Get current sphere from queue
    Get a particle radius
    Get neighbor spheres
    Get candidate point list for possible new sphere placement
    Remove candidates that intersect any neighboring spheres or boundary
    Get valid points
    if Number of valid points > 0 then
        Get best closest point to current sphere and generate sphere with selected radius
        Add new sphere to queue
        Decrease count for particle type by 1
    end
    if Number of valid points < 2 then
        Remove current sphere from queue
    end
end
```

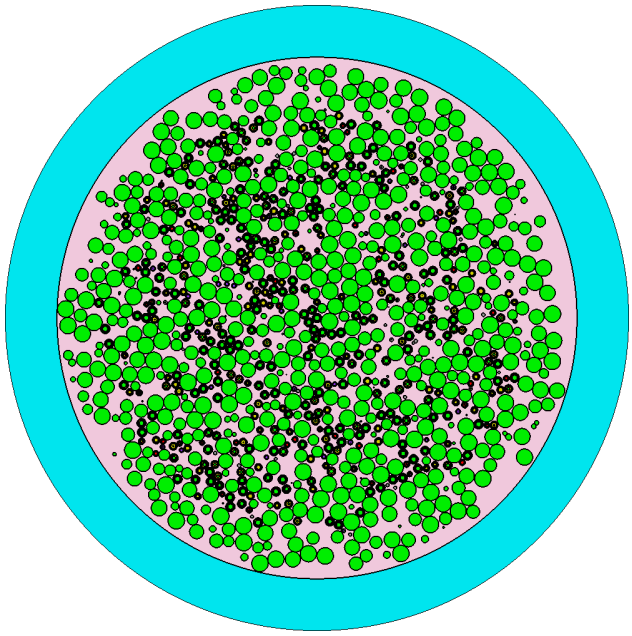

Figure 25. A pebble packed with two differently sized TRISO particles to achieve a packing fraction of 52%.

3.4 ONGOING AND FUTURE WORK

Future `Titan` development plans include the following.

1. Continue sphere-packing work to achieve high packing fractions in spherical shells, cylinders, and cylindrical shells.
2. Add support for the following units:
   - Boiling water reactor (BWR) Control Blades
   - Generic Pin
   - Ring Map (Canadian Deuterium Uranium (CANDU)-style assembly)
   - MSRE Stringer
   - Core Baffle
   - Control Drum
   - Channel Box
   - Pebble Bed Hopper
   - Generic Union Unit
3. Add support for `Shift` macroscopic *CELLNODAL* tallies for cross section generation.

4. GPBR EQUILIBRIUM CORE MODELING

Based on recent modeling and simulation efforts at INL [9–12], a `Shift` model of a 200 MWth GPBR was developed. `Shift` was applied through the `Omnibus` frontend using an ORANGE model. Using the ORANGE geometry enabled the use of recent enhancements for PBR modeling, as reported in previous work by the authors [13]. The following sections cover additions to the ORANGE geometry implemented for the GPBR modeling effort, the developed `Shift` GPBR model, the application of INL's capabilities for equilibrium core search, and ideas for future work supporting PBR modeling with `Shift`.

4.1 ENABLING INTERSECTION AND UNION SHAPES IN ORANGE

Modeling of the GPBR requires the consideration of so-called *dimples* that cut into the reflector surrounding the cylindrical fuel region. These dimples are wall features that significantly reduce localized ordering of pebbles in the outer core regions and cause a more consistent pebble packing fraction in these regions during operation [14]. Figure 26 depicts the GPBR's lower fuel region without the surrounding reflector, indicating the dimples that extend across the fuel region into the reflector.

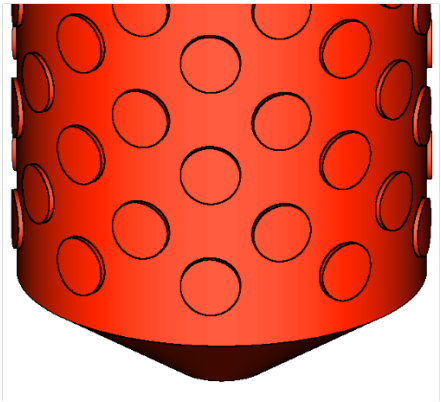

Figure 26. Lower fuel region in the GPBR model showing the dimples in the outer reflector.

Modeling of a dimple requires regions defined by the intersection of one cylinder with two other cylinders. Figure 27 shows a simplified model that indicates the cylinder with a small radius intersecting with two cylinders to form the red dimple region. Previously, the ORANGE geometry permitted the specification of various shapes, such as cylinders, and the placement of a material into a region defined by a list of intersecting shapes. Although it is possible to define a model with a single dimple region with a number of intersecting shapes, the full GPBR model includes 234 dimples, which made the geometry construction necessarily complex. In particular, this approach required the pebble region to be placed multiple times into different regions. Considering more than 200,000 pebbles in GPBR's core, this constraint provided a significant obstacle in the ORANGE GPBR model development.

To simplify the ORANGE GPBR geometry, new *intersection* and *union* shapes were introduced. Users can now create shapes that are formed by a list of intersecting shapes or by unionizing a list of shapes. Listing 7 provides an example use of these new shapes: the use of intersections and a union shape allows the definition of *one* shape that corresponds to the main core with all the dimples—that is, the complete region that is filled with pebbles.

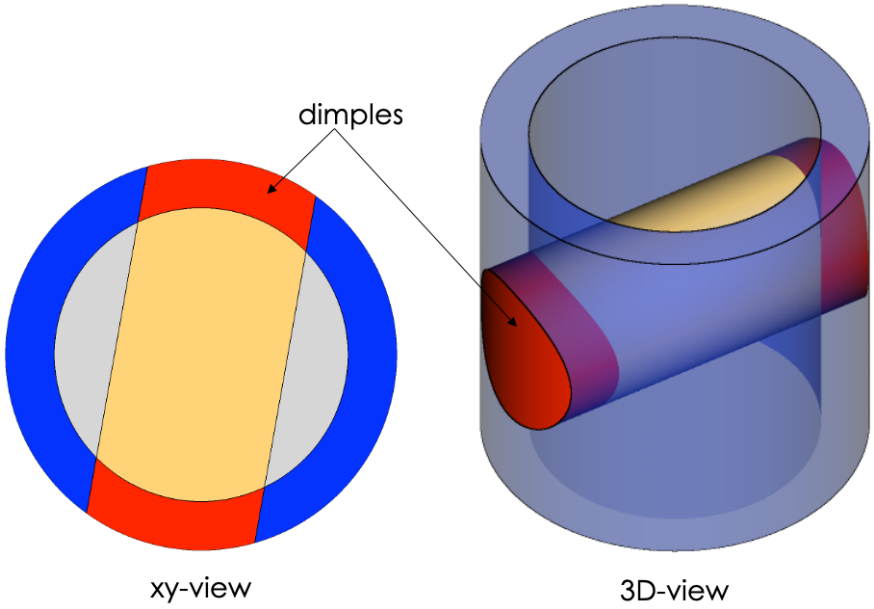

Figure 27. Simple model with intersecting cylinders to form a dimple.

Listing 7. ORANGE geometry of dimples using intersection and union shapes.

```
! main pebble cylinder
[..][SHAPE=cyl inner_cyl]
axis      z
extents   1.0 964.0
radius    120.0
! outer radius of dimples
[..][SHAPE=cyl outer_cyl]
axis      z
extents   1.0 964.0
radius    123.0

! small cylinders cutting into the reflector to form a dimple
[..][SHAPE=cyl cyl_1]
axis      x
extents   -150 150
radius    17.5
rotate    0.174 -0.985 0 0.985 0.174 0 0 0 1
origin    0.0 0.0 39.0
[..][SHAPE=cyl cyl_2]
axis      x
extents   -150 150
radius    17.5
rotate    0.174 -0.985 0 0.985 0.174 0 0 0 1
origin    0.0 0.0 108.99999999999999
[..][SHAPE=cyl cyl_3]
axis      x
extents   -150 150
radius    17.5
rotate    0.174 -0.985 0 0.985 0.174 0 0 0 1
origin    0.0 0.0 179.0

! intersection of shapes to form the dimple in the reflector
```

```
[..][SHAPE=intersection dimple_1]
shapes outer_cyl cyl_1
[..][SHAPE=intersection dimple_2]
shapes outer_cyl cyl_2
[..][SHAPE=intersection dimple_3]
shapes outer_cyl cyl_3

! union of all dimples and the main pebble cylinder
[..][SHAPE=union pebble_region]
shapes inner_cyl dimple_1 dimple_2 dimple_3

! material (or pebbles) conveniently placed within one shape
[..][CELL core]
comp   fuel
shapes pebble_region
```

4.2 SHIFT GPBR MODEL

Details of the GPBR design are described elsewhere [9–12]; only major design parameters are described here. The GPBR is designed for a power of 200 MWth. A cylindrical core with 1.2 m radius and 9 m height and the discharge cone contain approximately 220,000 fuel pebbles. The GPBR fuel pebble consists of a fuel zone that is 5 cm in diameter and contains 18,687 tristructural isotropic (TRISO) fuel particles distributed randomly in a graphite matrix. The fuel zone is surrounded by a 5 mm graphite layer, which results in a pebble with a 6 cm outer diameter. The TRISO packing fraction in the fuel region is approximately 9.344% and yields 7 g of uranium per pebble. During equilibrium core operation, the UCO fuel has a ^{235}U enrichment of 15.6 wt%. On average, each fuel pebble travels six times through the reactor core (referred to as six passes) before it reaches a maximum discharge burnup of 150 GWd/tU.

The ORANGE full core model (Figure 28), including geometry and material compositions, was developed based on a GPBR `Serpent` equilibrium core model that was kindly shared by INL. The fuel region is divided into five channels with multiple axial zones, resulting in 59 pebble regions. Each region contains a mixture of six different pebble types because each region contains pebbles at different passes through the core (i.e., different fuel compositions at different burnups). This results in 354 unique pebble definitions, with each unique pebble being found in one specific region only. Applying the capability for automatic random placement of TRISO particles within a fuel zone led to a unique TRISO particle distribution in each of the 354 unique pebbles. To improve runtime and make use of latest enhancements in ORANGE, the pebbles were placed at specific coordinates in the fuel region using ORANGE's *replica* capability [13], with the coordinates determined by INL using a Discrete Element Method (DEM) solver [14].

The GPBR model includes 18 riser, 9 control, and 9 safety rod channels. However, for all calculations performed here, the control and safety rods were fully withdrawn, and the riser channels did not include any pebbles.

Initial `Shift` calculations of the developed GPBR model were performed to troubleshoot the complex geometry, confirm the consistency of the `Shift` geometry with `Serpent` geometry, and determine run time and memory requirements for a single full-core calculation with tallies for depletion calculations enabled. For each full-core neutron transport calculation, 20,000 neutron histories per generation in 200 active and 40 inactive generations were simulated. For performance assessment, the memory and computation time for a single `Shift` full-core neutron transport calculation is compared with a corresponding `Serpent` calculation in Table 9. Both calculations were run on a single central processing unit (CPU) while reserving the full compute node. The `Serpent` calculation shows a significantly shorter run time, but a slightly larger memory footprint than `Shift` due to the use of Delta tracking. With a 5x increase in runtime compared to

Serpent and a slightly smaller memory footprint, the Shift result is still considered excellent given that the modeling and simulation of this complex model with both randomly distributed TRISO particles and randomly distributed pebbles was only recently made possible with the uniform grid accelerations [13].

Table 9. Comparison of Serpent and Shift performance for a GPBR neutron transport calculation.

Code	Memory per CPU [GB]	Runtime [CPU-hours]	Runtime [Particles/second]
Shift	8.5	131.7	10
Serpent	11.4	26.5	50

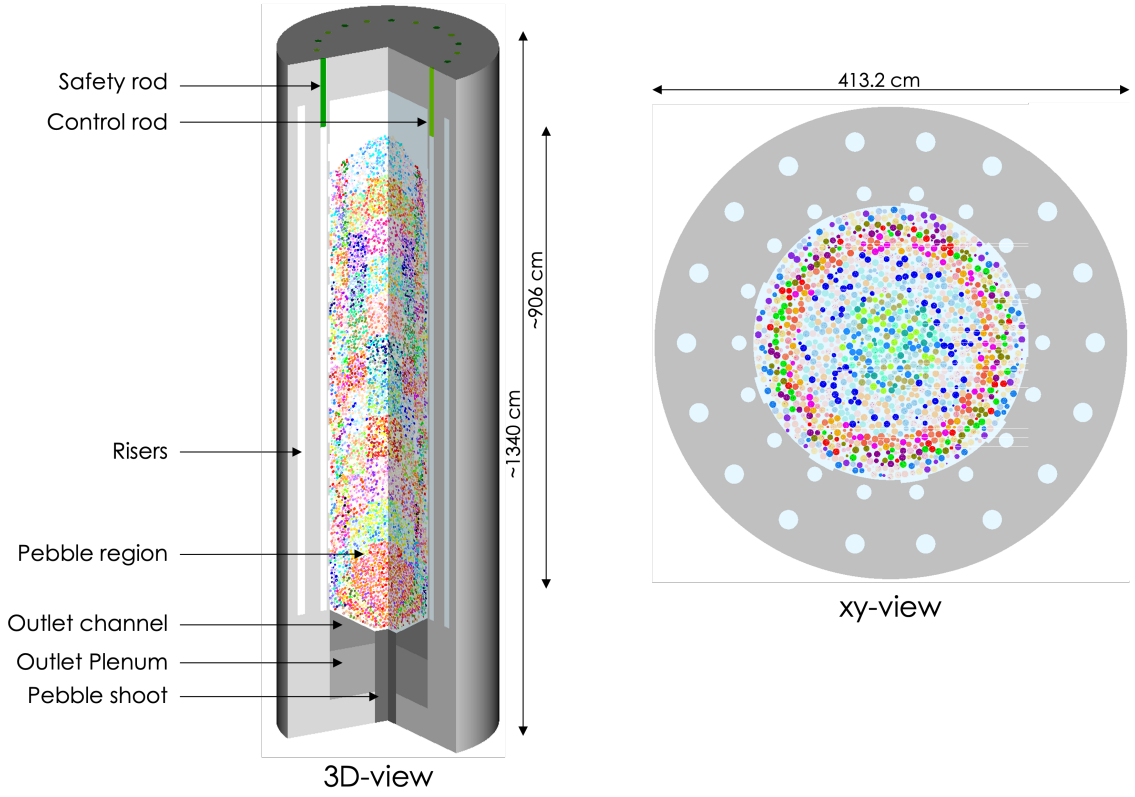

Figure 28. Shift GPBR full core model.

4.3 RUNNING-IN

PBRs operate the majority of their lifetime at a state of equilibrium. In an equilibrium core, the entire core consists of fuel pebbles at different levels of burnup. Fresh fuel pebbles are continuously added to the core, whereas fuel pebbles that have achieved the target discharge burnup are continuously removed from the core. Average conditions in any given region in the core—that is, region-average pebble burnup, fuel inventory, temperatures, etc.—are approximately constant. It is appropriate to assume that pebbles travel only axially through the core and that radial movement can be neglected. Since pebbles in the different radial regions of a core travel with different axial speed, radial zones should be considered in addition to axial zones when modeling a PBR.

In the GPBR equilibrium core, fuel pebbles travel on average 6 times through the core before they are discharged because they have reached their target discharge burnup. Pebbles are continuously added to the

top of the core, and they travel to the bottom. There, they are unloaded and their integrity and burnup is measured before they are either re-inserted into the core or discharged. Consequently, an axial zone in the core always includes a mixture of pebbles at 6 different passes. The closer an axial zone is to the bottom of the core, the higher the average pebble burnup in this zone.

The initial loading of a PBR is a mixture of fresh fuel pebbles at potentially different (lower) enrichments and graphite pebbles that do not contain any fuel. During the *running-in* phase, the graphite pebbles are continuously being replaced by fuel pebbles, and fuel pebbles are transitioned to fuel pebbles at the target equilibrium core enrichment. This running-in phase can take months to years, depending on the reactor.

To model an equilibrium core, one can either estimate the zone-wise pebble inventories at equilibrium directly via some iterative approach (*jump-in* approach), or one can simulate the running-in process. INL has developed Python scripts, named *kugelpy*, wrapped around the `Serpent` MC code to allow the determination of an equilibrium core through both the *jump-in* and the *running-in* approaches [9–12]. Based on a number of user input parameters (equilibrium fresh fuel compositions, startup fresh fuel compositions, power, temperature, etc.), these scripts manage the transition of fuel pebbles—or rather the transition of fuel compositions—from one zone to another after each depletion step. By continuously running full-core depletion calculations and moving the fuel compositions, the scripts simulate the running-in process. More details about *kugelpy* can be found elsewhere [9–12].

In this work, the INL team kindly shared their *kugelpy* scripts and allowed the ORNL team to test application of *kugelpy* in combination with `Serpent` on ORNL's computing clusters. Only minor script modifications related to the job submission on the cluster were needed to enable the successful application of the scripts with `Serpent`. As the next step, the *kugelpy* scripts were modified to allow execution with `Shift`. Due to larger differences in geometry construction between `Serpent` and `Shift`, the modifications in this first stage did not involve the automatic generation of the reactor's structural geometry; instead, the user must provide the structural geometry in a separate file. However, the fuel pebble composition management as well as the automatic execution of the neutron transport and depletion calculation were fully realized so that first equilibrium core calculations with *kugelpy*/`Shift` were successfully conducted. As examples of quantities to study during the running-in process, Figure 29 shows the input power, the full-core k_{eff} eigenvalue at the beginning of a depletion step, and the fraction of graphite pebbles remaining in the core as a function of time.

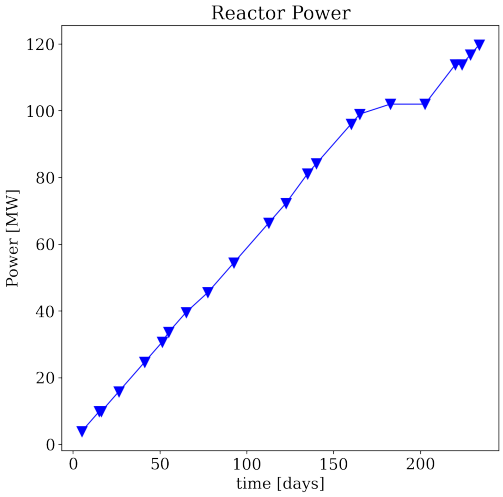

(a) Power (input)

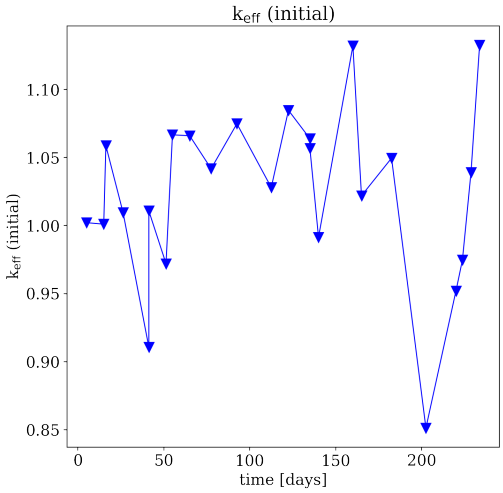

(b) k_{eff} at the beginning of a depletion step

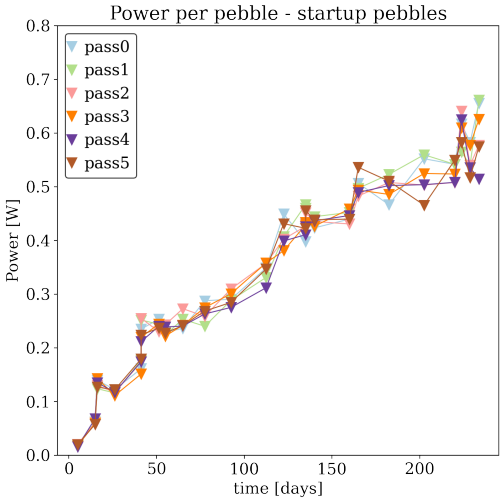

(c) Average power per pebble in the startup pebbles

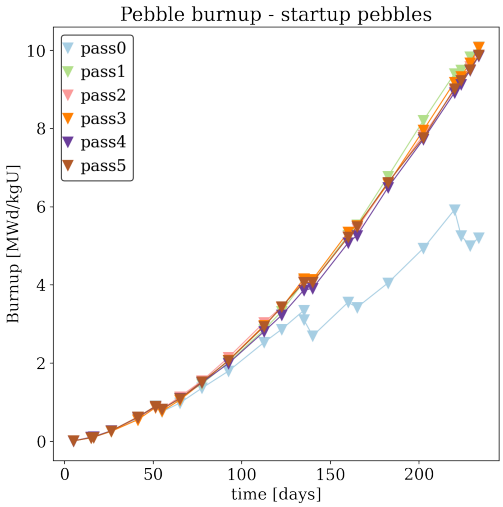

(d) Average burnup per pebble in the startup pebbles

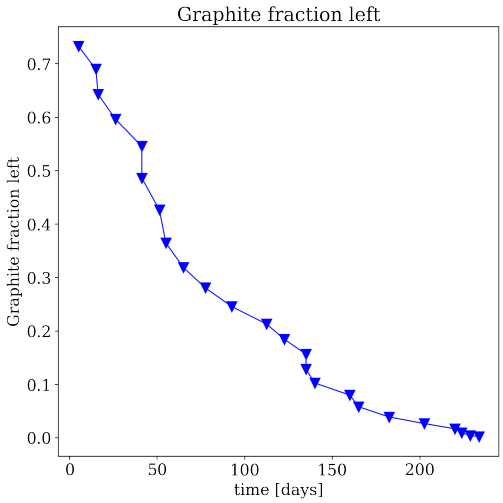

(e) Fraction of graphite pebbles in the core

Figure 29. Quantities of interest as a function of time during the GPBR running-in phase.

4.4 FUTURE WORK

Future work supporting the modeling and simulation of PBRs with `Shift` should involve the following items:

1. Fully automate PBR equilibrium core search with `Shift`. Only a part of the capabilities enabled with INL's *kugelpy* scripts have been enabled in this work for use with `Shift`. An automated process for `Shift` could continue adapting INL's *kugelpy* scripts to `Shift`, build upon a recently developed iteration process for jump-in equilibrium core generation developed by ORNL [15], or be based on a new approach.
2. Perform sensitivity studies in the equilibrium core search with respect to relevant depletion parameters such as the predictor–corrector methods. This worked used a simple procedure with one predictor sub-step, keeping the pebbles at static locations during the procedure. Given the slow travel of the pebbles from one axial zone to another, the consideration of pebble movement in the predictor–corrector procedure should be studied.
3. Make determination of multiple sets of TRISO coordinates for multiple unique pebbles more efficient by (1) permitting one automatically determined random distribution to be used in multiple pebble definitions and (2) parallelizing determination of random distributions for multiple pebbles (scatter multiple calls to the generation of random distribution across processors).
4. Enable determination of coordinates for fuel pebbles in a PBR core with a DEM solver or other capability. This work leveraged pebble coordinates determined by INL using a DEM solver.
5. Enable restart of all nuclide densities in depletion calculations from previous depletion calculations. The depletion and decay solver Oak Ridge Isotope Generator (ORIGEN) tracks 1,675 nuclides. Compositions in a `Shift` model may only include nuclides that are available in the CE nuclear data library (422 nuclides in the case of the ENDF/B-VII.1 library). If a depletion calculation is restarted, then compositions are initiated with the densities from the previous depletion calculations. Because densities can only be provided for the nuclides in the CE library, all other nuclides are not correctly restarted and begin with a zero density, which may cause a small bias in results.

5. CONCLUSIONS AND FUTURE WORK

This report documents FY23 modeling enhancements to Titan and Shift, multigroup cross section enhancements to Shift, and the demonstration of an equilibrium code search of a generic PBR with Shift. To facilitate collaboration under NEAMS, the process of releasing beta versions of SCALE to collaborators under a GU-EULA was undertaken and is almost complete.

Titan now supports more concrete unit types, cell tallies, and high packing fraction modeling for sphere-packed pebbles. These new features focus on ease of usability and automation for modeling advanced reactor systems. The algorithm implemented for sphere-packed pebble packing can achieve efficient packing of fractions greater than 52%.

Shift multigroup cross section capabilities now support calculation of energy deposition, neutron velocity, and kinetics parameters as well as the ability to run a prompt eigenvalue calculation. Computational validation of the prompt eigenvalue capability was performed between KENO and Shift for a 2D MSRE pincell, which yielded very good agreement between tallied and calculated k_{eff} and β_{eff}. Analysis of the applicability of higher-order scattering cross section moments generated by Shift was performed using a 3D ABTR pincell. It was found that cross sections for this problem agreed well between Shift and Serpent, but a future area of research is analysis of the accuracy of higher-order scattering moments when weighting by flux moments.

Finally, an initial demonstration of an equilibrium core search of a generic PBR, GPBR, using Shift was shown by using and adapting INL's *kugelpy*, which is a Python program initially only wrapped around the Serpent MC code to perform an equilibrium core search through both the *jump-in* and the *running-in* approaches. This entailed developing a detailed SCALE GPBR model with both randomly distributed TRISO particles and randomly distributed pebbles in the core, making use of the latest modeling enhancements in Shift for TRISO systems.

5.1 FUTURE WORK

Specific future areas of research are outlined in Sections 2.4, 3.4, and 4.4. A brief summary of these topics is reiterated here.

- Multigroup cross section generation with Shift:
  1. Tally and calculate the delayed neutron spectrum.
  2. Weight higher-order scattering matrices by higher-order flux moments.
  3. Produce microscopic cross sections.
  4. Allow scaling of scalar flux and relevant cross sections (such as $\kappa_{fission}$) by a user-input power level.
  5. Add adjoint-weighted kinetics parameters.
- Titan enhancements:
  1. Continue sphere-packing optimization to achieve high packing fractions in spherical shells, cylinders, and cylindrical shells.
  2. Add support for more geometry units.
  3. Integrate macroscopic *CELLNODAL* tallies for cross section generation.

- PBR modeling and analysis with `Shift`:
    1. Fully automate PBR equilibrium core search with `Shift`.
    2. Perform sensitivity studies in the equilibrium core search with respect to relevant depletion parameters such as the predictor–corrector methods.
    3. Make determination of multiple sets of TRISO coordinates for multiple unique pebbles more efficient.
    4. Enable determination of coordinates for fuel pebbles in a PBR core with a DEM solver or other capability.
    5. Enable restart of all nuclide densities in depletion calculations from previous depletion calculations.

Other future efforts regarding MC modeling and simulation for advanced reactor systems should include the following:

1. Perform a pin power reconstruction calculation with `Shift` and `Griffin` by following the previous calculation and tutorial developed using `Serpent` and `Griffin` from Shikhar Kumar at ANL.
2. Add the capability to tally on a user-given mesh overlay.

6. ACKNOWLEDGMENTS

The authors would like to thank the `Griffin` developers and users, especially Javier Ortensi, for their invaluable assistance. The development of the GPBR equilibrium core with Shift leveraged the *kugelpy* capabilities and the `Serpent` full core developed by Ryan Stewart (INL) and Paolo Balestra (INL); their cooperation is much appreciated.

Thanks to Kyoung Lee for sharing his MSRE pincell inputs.

Thanks to 2023 ORNL summer interns, Maximilliano Velasco from North Carolina State University and Patrick Myers from University of Michigan, for assistance with testing and comparing cross sections generated with `Shift` and `Serpent`. These interns helped identify several issues with the cross section generation that were fixed in FY23, as detailed in the report.

Many thanks to Robert Lefebvre for his efforts in drafting the GU-EULA and putting `SCALE` through the copyright process.

This research made use of Idaho National Laboratory computing resources which are supported by the Office of Nuclear Energy of the US Department of Energy and the Nuclear Science User Facilities under Contract No. DE-AC07-05ID14517.

REFERENCES

[1] Tara Pandya, Friederike Bostelmann, Matthew A. Jessee, and Javier Ortensi. Two-step neutronics calculations with Shift and Griffin for advanced reactor systems. *Annals of Nuclear Energy*, 173(1), August 2022.

[2] Kang Seog Kim, Kevin T. Clarno, Yuxuan Liu, Xinyan Wang, William R. Martin, and Benjamin S. Collins. Neutron capture energies for flux normalization and approximate model for gamma-smeared power. Technical Report ORNL/SPR-2017/471, Oak Ridge National Laboratory, 9 2018.

[3] William A. Wieselquist and R. A. Lefebvre. SCALE 6.3.1 User Manual. Technical Report ORNL/TM-SCALE-6.3.1, Oak Ridge National Laboratory, Oak Ridge, TN, 2023.

[4] Dan Cacuci. *Handbook of Nuclear Engineering*. Springer New York, New York, 2010.

[5] MM Bretscher. Evaluation of reactor kinetic parameters without the need for perturbation codes. In *International Meeting on Reduced Enrichment for Research and Test Reactors (RERTR)*, 1997.

[6] R C. Robertson. Msre design & operations report part 1 description of reactor design. Technical Report ORNL-TM-728, Oak Ridge National Laboratory, 12 1965.

[7] Taek K. Kim. Benchmark specification of advanced burner test reactor. Technical Report ANL/NSE-20/65, Argonne National Laboratory, 12 2020.

[8] Elias Lozano, Deane Roehl, Waldemar Celes, and Marcelo Gattass. An efficient algorithm to generate random sphere packs in arbitrary domains. *Computers & Mathematics with Applications*, 71(8):1586–1601, 2016.

[9] R. Stewart, P. Balestra, D.Reger, and G. Strydom. Novel pebble shuffling capabilities to generate reduced order models training databases. Technical Report INL/RPT-22-68918, Idaho National Laboratory, Idaho Falls, ID, 2022.

[10] R. Stewart, J. Cavaluzzi, P. Balestra, and G. Strydom. Establishing a methodology for performing a multiphysics run-in analysis of the gpbr200. Technical Report INL/RPT-23-74375, Idaho National Laboratory, Idaho Falls, ID, 2023.

[11] R. Stewart, D.Reger, P. Balestra, and G. Strydom. Methodology for Determining the Run-In Scenario for a Pebble Bed Reactor. In *Transactions of the American Nuclear Society, Vol. 127*, pages 412–415, 2022.

[12] R. Stewart, P. Balestra, D.Reger, E. Merzari, and G. Strydom. High-fidelity simulations of the run-in process for a pebble-bed reactor. *Annals of Nuclear Energy*, (submitted), 2023.

[13] Tara Pandya, Friederike Bostelmann, Matthew A. Jessee, Tarek Ghaddar, Philip Britt, and Seth Johnson. Modeling, Performance Assessment, and Nodal Data Analysis of TRISO- Fueled Systems with Shift. Technical Report ORNL/TM-2022/2601, Oak Ridge National Laboratory, Oak Ridge, TN, 2022.

[14] David Reger, Elia Merzari, Paolo Balestra, Ryan Stewart, and Gerhard Strydom. Energy Discrete element simulation of Pebble Bed Reactors on graphics processing units. *Annals of Nuclear Energy*, 190:109896, 2023.

[15] Friederike Bostelmann, Cihangar Celik, Robert Kile, and William Wieselquist. SCALE Analysis of a Fluoride Salt Cooled High Temperature Reactor in Support of Severe Accident Analysis. Technical report, Oak Ridge National Laboratory, 2021.

APPENDIX A. MSRE 2D PINCELL INPUTS

APPENDIX A. MSRE 2D PINCELL INPUTS

Listing A.1. SCALE 2D MSRE Pincell Input

```
=csas6
MSRE 2D
ce_v7.1_endf

read comp
' Graphite, density 1.8492 g/cc (specs: 1.8507 g/cc)
  c-graphite  6    0    9.27998E-02    922.0389    end
' Fuel salt, density 2.2858347 g/cc (specs: 2.3275 g/cc)
  li-6       10    0    1.59545E-06    922.0389    end
  li-7       10    0    2.15584E-02    922.0389    end
  be-9       10    0    9.68537E-03    922.0389    end
  zr         10    0    1.65854E-03    922.0389    end
  u-234      10    0    7.96059E-07    922.0389    end
  u-235      10    0    9.28736E-05    922.0389    end
  u-236      10    0    7.96060E-07    922.0389    end
  u-238      10    0    1.70887E-04    922.0389    end
  f-19       10    0    4.86265E-02    922.0389    end
end comp

read parameters
pnu=yes
npg=500000
nsk=50
gen=500
htm=no
plt=no
end parameters

read geometry
' ++++++++++++++++++++++++++++++++++++++++++++++++++++++++++++++++++++++
'                     FUEL ELEMENT UNITS
' ++++++++++++++++++++++++++++++++++++++++++++++++++++++++++++++++++++++
' fuel stringer block
global unit 10
' inner and outer cuboid
  cuboid   10  4p2.54 2p0.5
  cuboid   11  4p2.032 2p0.5
' cylinders: upper and lower

  cylinder 21  0.508 2p0.5 origin x=-1.016 y= 2.54 com="upper left"
  cylinder 22  0.508 2p0.5 origin x= 1.016 y= 2.54 com="upper right"
  cylinder 23  0.508 2p0.5 origin x=-1.016 y=-2.54 com="lower left"
  cylinder 24  0.508 2p0.5 origin x= 1.016 y=-2.54 com="lower left"
' cylinders: left and right
  cylinder 25  0.508 2p0.5 origin x= 2.54 y= 1.016 com="right up"
  cylinder 26  0.508 2p0.5 origin x= 2.54 y=-1.016 com="right down"
  cylinder 27  0.508 2p0.5 origin x=-2.54 y= 1.016 com="left up"
  cylinder 28  0.508 2p0.5 origin x=-2.54 y=-1.016 com="left down"
' salt cuboids
  cuboid   31  2.54  2.032  2p1.016 2p0.5 com="right"
  cuboid   32 -2.032 -2.54  2p1.016 2p0.5 com="left"
  cuboid   33  2p1.016  2.540  2.032 2p0.5 com="upper"
  cuboid   34  2p1.016 -2.032 -2.54 2p0.5 com="lower"
' center graphite
  media  6 1  11 vol=16.516096
```

```
' outer graphite
  media  6 1  10 -11 -21 -22 -23 -24 -25 -26 -27 -28 -31 -32 -33 -34 vol=3.539816067
' salt in cylinders
  media 10 1 -11 10 21 -33 vol=0.202682992
  media 10 1 -11 10 22 -33 vol=0.202682992
  media 10 1 -11 10 23 -34 vol=0.202682992
  media 10 1 -11 10 24 -34 vol=0.202682992
  media 10 1 -11 10 25 -31 vol=0.202682992
  media 10 1 -11 10 26 -31 vol=0.202682992
  media 10 1 -11 10 27 -32 vol=0.202682992
  media 10 1 -11 10 28 -32 vol=0.202682992
' salt in cuboids
  media 10 1 31 vol=1.032256
  media 10 1 32 vol=1.032256
  media 10 1 33 vol=1.032256
  media 10 1 34 vol=1.032256
  boundary 10
end geometry

read bounds
   all=mirror
end bounds

read volume
type=trace nrays=10000
end volume

end data
end
```

Listing A.2. Shift 2D MSRE Pincell Input

```
[PROBLEM]
name "MSRE 2D"
mode kcode

[MODEL=scale]
input "msre.inp"

[PHYSICS=ce]
ce_lib ce_v7.1_endf
! broaden to desired temperature
[PHYSICS][BROADEN]
kinematics true

[TALLY]

[TALLY][CELLNODAL all]
coarse_neutron_bins 2.0000e+07 1.7330e+07 1.5680e+07 1.4550e+07 1.3840e+07 1.2840e+07
             1.0000e+07 8.1870e+06 6.4340e+06 4.8000e+06 4.3040e+06 3.0000e+06
             2.4790e+06 2.3540e+06 1.8500e+06 1.5000e+06 1.4000e+06 1.3530e+06
             1.3170e+06 1.2500e+06 1.2000e+06 1.1000e+06 1.0100e+06 9.2000e+05
             9.0000e+05 8.7500e+05 8.6110e+05 8.2000e+05 7.5000e+05 6.7900e+05
             6.7000e+05 6.0000e+05 5.7300e+05 5.5000e+05 5.0000e+05 4.7000e+05
             4.4000e+05 4.2000e+05 4.0000e+05 3.3000e+05 2.7000e+05 1.8300e+05
             1.4900e+05 1.2830e+05 1.0000e+05 8.5000e+04 8.2000e+04 7.5000e+04
             7.3000e+04 6.0000e+04 5.2000e+04 5.0000e+04 4.5000e+04 3.0000e+04
             2.0000e+04 1.7000e+04 1.3000e+04 9.1180e+03 8.0300e+03 5.7000e+03
             3.9000e+03 3.7400e+03 3.0000e+03 2.5000e+03 2.2500e+03 2.2000e+03
```

```
                1.8000e+03 1.5500e+03 1.5000e+03 1.1500e+03 9.5000e+02 6.8300e+02
                6.7000e+02 5.5000e+02 3.0500e+02 2.8500e+02 2.4000e+02 2.2000e+02
                2.0950e+02 2.0740e+02 2.0200e+02 1.9300e+02 1.9150e+02 1.8850e+02
                1.8770e+02 1.8000e+02 1.7000e+02 1.4873e+02 1.2200e+02 1.1900e+02
                1.1750e+02 1.1600e+02 1.1300e+02 1.0800e+02 1.0500e+02 1.0120e+02
                9.7000e+01 9.0000e+01 8.1700e+01 8.0000e+01 7.6000e+01 7.2000e+01
                6.7500e+01 6.5000e+01 6.3000e+01 6.1000e+01 5.8000e+01 5.3400e+01
                5.0600e+01 4.8300e+01 4.5200e+01 4.4000e+01 4.2400e+01 4.1000e+01
                3.9600e+01 3.9100e+01 3.8000e+01 3.7630e+01 3.7270e+01 3.7130e+01
                3.7000e+01 3.6000e+01 3.5500e+01 3.5000e+01 3.3750e+01 3.3250e+01
                3.1750e+01 3.1250e+01 3.0000e+01 2.7500e+01 2.5000e+01 2.2500e+01
                2.1750e+01 2.1200e+01 2.0500e+01 2.0000e+01 1.9400e+01 1.8500e+01
                1.7000e+01 1.6000e+01 1.4400e+01 1.2900e+01 1.1900e+01 1.1500e+01
                1.0000e+01 9.1000e+00 8.1000e+00 7.1500e+00 7.0000e+00 6.8750e+00
                6.7500e+00 6.5000e+00 6.2500e+00 6.0000e+00 5.4000e+00 5.0000e+00
                4.7000e+00 4.0000e+00 3.7300e+00 3.5000e+00 3.2000e+00 3.1000e+00
                3.0000e+00 2.9700e+00 2.8700e+00 2.7700e+00 2.6700e+00 2.5700e+00
                2.4700e+00 2.3800e+00 2.3000e+00 2.2100e+00 2.1200e+00 2.0000e+00
                1.9400e+00 1.8600e+00 1.7700e+00 1.6800e+00 1.5900e+00 1.5000e+00
                1.4500e+00 1.4000e+00 1.3500e+00 1.3000e+00 1.2500e+00 1.2250e+00
                1.2000e+00 1.1750e+00 1.1500e+00 1.1400e+00 1.1300e+00 1.1200e+00
                1.1100e+00 1.1000e+00 1.0900e+00 1.0800e+00 1.0700e+00 1.0600e+00
                1.0500e+00 1.0400e+00 1.0300e+00 1.0200e+00 1.0100e+00 1.0000e+00
                9.7500e-01 9.5000e-01 9.2500e-01 9.0000e-01 8.5000e-01 8.0000e-01
                7.5000e-01 7.0000e-01 6.5000e-01 6.2500e-01 6.0000e-01 5.5000e-01
                5.0000e-01 4.5000e-01 4.0000e-01 3.7500e-01 3.5000e-01 3.2500e-01
                3.0000e-01 2.7500e-01 2.5000e-01 2.2500e-01 2.0000e-01 1.8000e-01
                1.5000e-01 1.2500e-01 1.0000e-01 9.0000e-02 8.0000e-02 7.0000e-02
                6.0000e-02 5.0000e-02 4.0000e-02 3.0000e-02 2.5300e-02 1.0000e-02
                7.5000e-03 5.0000e-03 4.0000e-03 3.0000e-03 2.5000e-03 2.0000e-03
                1.5000e-03 1.2000e-03 1.0000e-03 7.5000e-04 5.0000e-04 1.0000e-04
                1.0000e-05
cells_by_homog  "10.1":"10.2":"10.3":"10.4":"10.5":"10.6":"10.7":"10.8":"10.9":"10.10" \
                 :"10.11":"10.12":"10.13":"10.14"
calculate_kinetics true

[SHIFT]

[SHIFT][KCODE]
initial_keff 1.0
num_histories_per_cycle 500000
num_cycles 500
num_inactive_cycles 50
prompt_only true

[OUTPUT]
display_counter false
```

APPENDIX B. ABTR 3D PINCELL INPUTS

APPENDIX B. ABTR 3D PINCELL INPUTS

Listing B.1. SCALE ABTR Input

```
' https://publications.anl.gov/anlpubs/2021/01/164846.pdf
=csas6
ABTR250 - 3D fuel pin
ce_v7.1_endf
read composition
' FUEL
Zr-90     1 0 3.752660e-03 855.65 end
Zr-91     1 0 8.183643e-04 855.65 end
Zr-92     1 0 1.250887e-03 855.65 end
Zr-94     1 0 1.267662e-03 855.65 end
Zr-96     1 0 2.042264e-04 855.65 end
Mo-92     1 0 1.441734e-04 855.65 end
Mo-94     1 0 9.009613e-05 855.65 end
Mo-95     1 0 1.552035e-04 855.65 end
Mo-96     1 0 1.628173e-04 855.65 end
Mo-97     1 0 9.331737e-05 855.65 end
Mo-98     1 0 2.361241e-04 855.65 end
Mo-100    1 0 9.439109e-05 855.65 end
 U-234    1 0 1.222500e-08 855.65 end
 U-235    1 0 3.224800e-05 855.65 end
 U-236    1 0 2.056100e-06 855.65 end
 U-238    1 0 2.022200e-02 855.65 end
Np-237    1 0 3.838700e-06 855.65 end
Pu-236    1 0 1.391800e-11 855.65 end
Pu-238    1 0 9.585400e-07 855.65 end
Pu-239    1 0 3.499100e-03 855.65 end
Pu-240    1 0 3.739800e-04 855.65 end
Pu-241    1 0 2.453500e-05 855.65 end
Pu-242    1 0 1.754200e-06 855.65 end
Am-241    1 0 1.420900e-06 855.65 end
Am-243    1 0 6.133800e-08 855.65 end
Cm-242    1 0 4.708300e-08 855.65 end
Cm-243    1 0 7.413800e-10 855.65 end
Cm-244    1 0 4.830500e-09 855.65 end
Cm-245    1 0 1.906400e-10 855.65 end
Cm-246    1 0 2.611200e-12 855.65 end
Am-242m   1 0 2.847500e-08 855.65 end
' COOL/BOND
Na-23     2 0 2.227200e-02 855.65 end
' GAP
He-3      3 0 2.448515e-11 855.65 end
He-4      3 0 2.459997e-05 855.65 end
' CLAD
Cr-50     4 0 4.512283e-04 855.65 end
Cr-52     4 0 8.701488e-03 855.65 end
Cr-53     4 0 9.866789e-04 855.65 end
Cr-54     4 0 2.456052e-04 855.65 end
Mn-55     4 0 4.600700e-04 855.65 end
Fe-54     4 0 4.082382e-03 855.65 end
Fe-56     4 0 6.408467e-02 855.65 end
Fe-57     4 0 1.479994e-03 855.65 end
Fe-58     4 0 1.969598e-04 855.65 end
Ni-58     4 0 2.931596e-04 855.65 end
Ni-60     4 0 1.129246e-04 855.65 end
Ni-61     4 0 4.908751e-06 855.65 end
```

```
Ni-62     4 0 1.565125e-05 855.65 end
Ni-64     4 0 3.985914e-06 855.65 end
Mo-92     4 0 7.251626e-05 855.65 end
Mo-94     4 0 4.531652e-05 855.65 end
Mo-95     4 0 7.806421e-05 855.65 end
Mo-96     4 0 8.189378e-05 855.65 end
Mo-97     4 0 4.693673e-05 855.65 end
Mo-98     4 0 1.187656e-04 855.65 end
Mo-100    4 0 4.747679e-05 855.65 end
' REFL
Na-23     5 0 1.559100e-02 855.65 end
Cr-50     5 0 1.405825e-04 855.65 end
Cr-52     5 0 2.710993e-03 855.65 end
Cr-53     5 0 3.074049e-04 855.65 end
Cr-54     5 0 7.651957e-05 855.65 end
Mn-55     5 0 5.084600e-04 855.65 end
Fe-54     5 0 9.280691e-04 855.65 end
Fe-56     5 0 1.456870e-02 855.65 end
Fe-57     5 0 3.364547e-04 855.65 end
Fe-58     5 0 4.477590e-05 855.65 end
Ni-58     5 0 2.219579e-03 855.65 end
Ni-60     5 0 8.549781e-04 855.65 end
Ni-61     5 0 3.716530e-05 855.65 end
Ni-62     5 0 1.184992e-04 855.65 end
Ni-64     5 0 3.017829e-05 855.65 end
Mo-92     5 0 6.428495e-05 855.65 end
Mo-94     5 0 4.017265e-05 855.65 end
Mo-95     5 0 6.920315e-05 855.65 end
Mo-96     5 0 7.259803e-05 855.65 end
Mo-97     5 0 4.160895e-05 855.65 end
Mo-98     5 0 1.052846e-04 855.65 end
Mo-100    5 0 4.208770e-05 855.65 end
end composition

read geometry

global unit 1
'   Area of hexprism w/ apothem a is 2*a*a*sqrt3=0.722525
'   Lower struct
    hexprism  1 0.4567 50.24  0
    media 5 1 1 vol=36.2997
'   Lower reflector
    cylinder  2 0.4057 110.533 50.24
    hexprism  3 0.4567 110.533 50.24
    media 4 1 2    vol=31.1765
    media 2 1 3 -2 vol=12.3867
'   Fuel
    cylinder  4 0.3501 194.9438 110.533
    cylinder  5 0.4057 194.9438 110.533
    hexprism  6 0.4567 194.9438 110.533
    media 1 1 4    vol=32.5036
    media 4 1 5 -4 vol=11.1438
    media 2 1 6 -5 vol=17.3415
'   Sodium Bond
    cylinder  7 0.3501 214.7075 194.9438
    cylinder  8 0.4057 214.7075 194.9438
    hexprism  9 0.4567 214.7075 194.9438
    media 2 1 7    vol=7.61031
    media 4 1 8 -7 vol=2.60915
```

```
    media 2 1 9 -8 vol=4.06031
'   Plenum
    cylinder 10 0.3501 311.513 214.7075
    cylinder 11 0.4057 311.513 214.7075
    hexprism 12 0.4567 311.513 214.7075
    media 3 1 10    vol=37.2764
    media 4 1 11 -10 vol=12.78
    media 2 1 12 -11 vol=19.888
'   Upper struct
    hexprism 13 0.4567 341.663 311.513
    media 5 1 13 vol=21.7841
'   Boundary
    hexprism 14 0.4567 341.663 0
    boundary 14

end geometry
read bounds
 surface(1)=refl surface(2)=refl surface(3)=refl surface(4)=refl surface(5)=refl
 surface(6)=refl surface(7)=vacuum surface(8)=vacuum
end bounds
end data
end
```

Listing B.2. Shift 9-Group ABTR Input

```
[PROBLEM]
name "ABTR250 - 3D fuel pin"
mode kcode

[MODEL=scale]
input "../csas.inp"

[PHYSICS=ce]
ce_lib ce_v7.1_endf
dbrc False

! broaden to desired temperature
[PHYSICS][BROADEN]
kinematics true

[SOURCE=separable global_fission]
fissionable_only True

[SOURCE][SHAPE=box]
box -0.3501 0.3501 -0.3501 0.3501 110.533 194.9438

! [COMP]
! sclib_path '/Users/Shared/build/7.0b05/INSTALL/data/scale.rev40.sclib'

[TALLY]

[TALLY][CELLNODAL anl_9g]
fine_neutron_bins   1.419E+07   1.179E+07   9.802E+06   8.147E+06   6.771E+06
                    5.627E+06   4.677E+06   3.887E+06   3.230E+06   2.685E+06
                    2.231E+06   2.019E+06   1.827E+06   1.653E+06   1.496E+06
                    1.353E+06   1.225E+06   1.108E+06   1.003E+06   9.072E+05
                    8.208E+05   7.065E+05   6.081E+05   5.234E+05   4.505E+05
                    3.877E+05   3.337E+05   2.873E+05   2.472E+05   2.128E+05
                    1.832E+05   1.576E+05   1.357E+05   1.168E+05   1.005E+05
```

```
                    8.652E+04   7.447E+04   6.409E+04   5.517E+04   4.748E+04
                    4.087E+04   3.518E+04   3.028E+04   2.606E+04   2.243E+04
                    1.930E+04   1.662E+04   1.430E+04   1.231E+04   1.059E+04
                    9.119E+03   7.849E+03   6.755E+03   5.814E+03   5.005E+03
                    4.307E+03   3.707E+03   3.191E+03   2.747E+03   2.364E+03
                    2.035E+03   1.751E+03   1.507E+03   1.297E+03   1.117E+03
                    9.611E+02   8.272E+02   7.120E+02   6.128E+02   5.275E+02
                    4.540E+02   2.895E+02   1.846E+02   1.177E+02   7.505E+01
                    4.785E+01   3.051E+01   1.945E+01   1.241E+01   7.910E+00
                    5.043E+00   1.357E+00   3.649E-01   9.815E-02   2.640E-02
                    7.102E-03   1.910E-03   5.138E-04   1.382E-04   3.718E-05
                    1.000E-05

coarse_neutron_bins 1.419E+07
                    2.231E+06
                    8.208E+05
                    1.832E+05
                    4.087E+04
                    9.119E+03
                    2.035E+03
                    4.540E+02
                    5.043E+00
                    1.000E-05

cells_by_homog "1.1"                          ! LOWER
               "1.2":"1.5":"1.8":"1.11"       ! CLAD
               "1.3":"1.6":"1.7":"1.9":"1.12" ! COOL
               "1.4"                          ! FUEL
               "1.10"                         ! GAP
               "1.13"                         ! UPPER

cells_for_hybrid_scatter_col "1.1":"1.13"                    ! REFL
                             "1.2":"1.5":"1.8":"1.11"        ! CLAD
                             "1.3":"1.6":"1.7":"1.9":"1.12"  ! COOL
                             "1.4"                           ! FUEL
                             "1.10"                          ! GAP

cells_for_hybrid_scatter_pl "1.1"                           ! LOWER
                            "1.2":"1.5":"1.8":"1.11"        ! CLAD
                            "1.3":"1.6":"1.7":"1.9":"1.12"  ! COOL
                            "1.4"                           ! FUEL
                            "1.10"                          ! GAP
                            "1.13"                          ! UPPER

pn_order 2
calculate_kinetics false

[SHIFT]

[SHIFT][KCODE]
num_histories_per_cycle 500000
initial_keff 1.0
num_cycles 650
num_inactive_cycles 50

[POST]
[POST][MG_XS]
mgxs_tally       "anl_9g"
xml_output_file  "griffin-xs"
```

```
xml_lib_name     "3dpin"
xml_lib_desc     "Shift-generated 3d pin library"
griffin_homog_cells 1 2 3 4 5 6

[RUN=pbs]
detach True
email  tut@ornl.gov
nodes  4
ppn    48
walltime "99:00:00"
```

Listing B.3. Serpent 9-Group ABTR Input

```
% https://publications.anl.gov/anlpubs/2021/01/164846.pdf

set title "3D ABTR rod model"

%%%%%%%%%%%%%%%%%%%%%%%%%%%%%%%%%%%%%%%%%%%%%%%%%%%%%%%%%%%%%%%%%%%%%%%
%   Options
%%%%%%%%%%%%%%%%%%%%%%%%%%%%%%%%%%%%%%%%%%%%%%%%%%%%%%%%%%%%%%%%%%%%%%%

% use p-tables
set ures 1

% boundary conditions (x/y/z): 1 = vacuum, 2 = reflective, 3 = periodic
set bc 2 2 1

% neutron settings
set pop 500000 600 50

% plots
plot 33 500 500 20  % plot xy plane, lower structure
plot 33 500 500 100 % plot xy plane, lower reflector
plot 33 500 500 150 % plot xy plane, fuel
plot 33 500 500 200 % plot xy plane, sodium bond
plot 33 500 500 300 % plot xy plane, plenum
plot 33 500 500 330 % plot xy plane, upper structure

% energy group structures
ene anl9 1 1.00E-11 5.0435E-06 4.5400E-04 2.0347E-03 9.1188E-03  4.0868E-02
           1.8316E-01 8.2085E-01 2.2313E+00 1.4191E+01
ene eq_leth_90g 1 1.000E-11
                  3.718E-11    1.382E-10    5.138E-10    1.910E-09    7.102E-09
                  2.640E-08    9.815E-08    3.649E-07    1.357E-06    5.043E-06
                  7.910E-06    1.241E-05    1.945E-05    3.051E-05    4.785E-05
                  7.505E-05    1.177E-04    1.846E-04    2.895E-04    4.540E-04
                  5.275E-04    6.128E-04    7.120E-04    8.272E-04    9.611E-04
                  1.117E-03    1.297E-03    1.507E-03    1.751E-03    2.035E-03
                  2.364E-03    2.747E-03    3.191E-03    3.707E-03    4.307E-03
                  5.005E-03    5.814E-03    6.755E-03    7.849E-03    9.119E-03
                  1.059E-02    1.231E-02    1.430E-02    1.662E-02    1.930E-02
                  2.243E-02    2.606E-02    3.028E-02    3.518E-02    4.087E-02
                  4.748E-02    5.517E-02    6.409E-02    7.447E-02    8.652E-02
                  1.005E-01    1.168E-01    1.357E-01    1.576E-01    1.832E-01
                  2.128E-01    2.472E-01    2.873E-01    3.337E-01    3.877E-01
                  4.505E-01    5.234E-01    6.081E-01    7.065E-01    8.208E-01
                  9.072E-01    1.003E+00    1.108E+00    1.225E+00    1.353E+00
                  1.496E+00    1.653E+00    1.827E+00    2.019E+00    2.231E+00
                  2.685E+00    3.230E+00    3.887E+00    4.677E+00    5.627E+00
```

```
                  6.771E+00    8.147E+00    9.802E+00    1.179E+01    1.419E+01

% generate few-group xs
set gcu 1001 1002 1003 1004 1005 1006
set micro eq_leth_90g
set nfg anl9

%%%%%%%%%%%%%%%%%%%%%%%%%%%%%%%%%%%%%%%%%%%%%%%%%%%%%%%%%%%%%%%%%%%%%%%
%   Materials
%%%%%%%%%%%%%%%%%%%%%%%%%%%%%%%%%%%%%%%%%%%%%%%%%%%%%%%%%%%%%%%%%%%%%%%

mat fuel sum tmp 855.65 rgb 255 0 0 % red
Zr-90.06c     3.752660e-03
Zr-91.06c     8.183643e-04
Zr-92.06c     1.250887e-03
Zr-94.06c     1.267662e-03
Zr-96.06c     2.042264e-04
Mo-92.06c     1.441734e-04
Mo-94.06c     9.009613e-05
Mo-95.06c     1.552035e-04
Mo-96.06c     1.628173e-04
Mo-97.06c     9.331737e-05
Mo-98.06c     2.361241e-04
Mo-100.06c    9.439109e-05
 U-234.06c    1.222500e-08
 U-235.06c    3.224800e-05
 U-236.06c    2.056100e-06
 U-238.06c    2.022200e-02
Np-237.06c    3.838700e-06
Pu-236.06c    1.391800e-11
Pu-238.06c    9.585400e-07
Pu-239.06c    3.499100e-03
Pu-240.06c    3.739800e-04
Pu-241.06c    2.453500e-05
Pu-242.06c    1.754200e-06
Am-241.06c    1.420900e-06
Am-243.06c    6.133800e-08
Cm-242.06c    4.708300e-08
Cm-243.06c    7.413800e-10
Cm-244.06c    4.830500e-09
Cm-245.06c    1.906400e-10
Cm-246.06c    2.611200e-12
Am-242m.06c   2.847500e-08

mat sodium sum tmp 855.65 rgb 255 255 0 % yellow
Na-23.06c     2.227200e-02

mat gap sum tmp 855.65     rgb 102 178 255 % light blue
He-3.06c      2.448515e-11
He-4.06c      2.459997e-05

mat clad sum tmp 855.65     rgb 192 192 192 % gray
Cr-50.06c     4.512283e-04
Cr-52.06c     8.701488e-03
Cr-53.06c     9.866789e-04
Cr-54.06c     2.456052e-04
Mn-55.06c     4.600700e-04
Fe-54.06c     4.082382e-03
Fe-56.06c     6.408467e-02
```

```
Fe-57.06c     1.479994e-03
Fe-58.06c     1.969598e-04
Ni-58.06c     2.931596e-04
Ni-60.06c     1.129246e-04
Ni-61.06c     4.908751e-06
Ni-62.06c     1.565125e-05
Ni-64.06c     3.985914e-06
Mo-92.06c     7.251626e-05
Mo-94.06c     4.531652e-05
Mo-95.06c     7.806421e-05
Mo-96.06c     8.189378e-05
Mo-97.06c     4.693673e-05
Mo-98.06c     1.187656e-04
Mo-100.06c    4.747679e-05

mat refl sum tmp 855.65      rgb 0 0 255 % blue
Na-23.06c     1.559100e-02
Cr-50.06c     1.405825e-04
Cr-52.06c     2.710993e-03
Cr-53.06c     3.074049e-04
Cr-54.06c     7.651957e-05
Mn-55.06c     5.084600e-04
Fe-54.06c     9.280691e-04
Fe-56.06c     1.456870e-02
Fe-57.06c     3.364547e-04
Fe-58.06c     4.477590e-05
Ni-58.06c     2.219579e-03
Ni-60.06c     8.549781e-04
Ni-61.06c     3.716530e-05
Ni-62.06c     1.184992e-04
Ni-64.06c     3.017829e-05
Mo-92.06c     6.428495e-05
Mo-94.06c     4.017265e-05
Mo-95.06c     6.920315e-05
Mo-96.06c     7.259803e-05
Mo-97.06c     4.160895e-05
Mo-98.06c     1.052846e-04
Mo-100.06c    4.208770e-05

%%%%%%%%%%%%%%%%%%%%%%%%%%%%%%%%%%%%%%%%%%%%%%%%%%%%%%%%%%%%%%%%%%%%%%%
%   Geometry
%%%%%%%%%%%%%%%%%%%%%%%%%%%%%%%%%%%%%%%%%%%%%%%%%%%%%%%%%%%%%%%%%%%%%%%

surf inf inf
surf  1 hexyprism 0.0 0.0 0.4567  0          50.24
surf  2 cyl       0.0 0.0 0.4057  50.24    110.533
surf  3 hexyprism 0.0 0.0 0.4567  50.24    110.533
surf  4 cyl       0.0 0.0 0.3501  110.533  194.9438
surf  5 cyl       0.0 0.0 0.4057  110.533  194.9438
surf  6 hexyprism 0.0 0.0 0.4567  110.533  194.9438
surf  7 cyl       0.0 0.0 0.3501  194.9438 214.7075
surf  8 cyl       0.0 0.0 0.4057  194.9438 214.7075
surf  9 hexyprism 0.0 0.0 0.4567  194.9438 214.7075
surf 10 cyl       0.0 0.0 0.3501  214.7075 311.513
surf 11 cyl       0.0 0.0 0.4057  214.7075 311.513
surf 12 hexyprism 0.0 0.0 0.4567  214.7075 311.513
surf 13 hexyprism 0.0 0.0 0.4567  311.513  341.663
surf 14 hexyprism 0.0 0.0 0.4567  0        341.663
```

```
cell u_fuel     1001 fuel   -inf
cell u_clad     1002 clad   -inf
cell u_sodium   1003 sodium -inf
cell u_gap      1004 gap    -inf
cell u_refl_low 1005 refl   -inf
cell u_refl_up  1006 refl   -inf

cell 10 0 fill 1005 -1        % Lower struct
cell 11 0 fill 1002 -2        % Lower reflector
cell 12 0 fill 1003 -3    2   % Lower reflector
cell 13 0 fill 1001 -4        % Fuel
cell 14 0 fill 1002 -5    4   % Fuel
cell 15 0 fill 1003 -6    5   % Fuel
cell 16 0 fill 1003 -7        % Sodium Bond
cell 17 0 fill 1002 -8    7   % Sodium Bond
cell 18 0 fill 1003 -9    8   % Sodium Bond
cell 19 0 fill 1004 -10       % Plenum
cell 20 0 fill 1002 -11  10   % Plenum
cell 21 0 fill 1003 -12  11   % Plenum
cell 22 0 fill 1006 -13       % Upper struct
cell 23 0 outside    14
```

Listing B.4. Griffin 9-Group ABTR Input

```
[Mesh]
   [pin_cell]
     type = PolygonConcentricCircleMeshGenerator
     num_sides = 6
     polygon_size = 0.4567
     num_sectors_per_side = '2 2 2 2 2 2'
     ring_radii = '.3501 .4057'
     ring_intervals = '1 1'
     ring_block_ids = '1 2'
     background_block_ids = 3
     preserve_volumes = on
     quad_center_elements = true
   []
   [extrude]
     type                = NonuniformMeshExtruderGenerator
     input               = pin_cell
     extrusion_vector    = '0 0 1'

     layer_thickness     = '5.0 5.0 5.0 5.0 5.0 5.0 5.0 5.0 5.0 5.24
                            5.0 5.0 5.0 5.0 5.0 5.0 5.0 5.0 5.0 5.0 5.0 5.293
                            5.0 5.0 5.0 5.0 5.0 5.0 5.0 5.0 5.0 5.0 5.0 5.0 5.0 5.0 5.0 5.0 4.4108
                            5.0 5.0 5.0 4.7637
                            5.0 5.0 5.0 5.0 5.0 5.0 5.0 5.0 5.0 5.0 5.0 5.0 5.0 5.0 5.0 5.0 5.4 5.4 5
                            5.0 5.0 5.0 5.0 5.0 5.15'
     #layer_thickness     = '50.24 60.293 84.4108 19.7637 96.8055 30.15'
     existing_subdomains = '1 2 3'
     layers              = '  0 1  2  3  4  5  6  7  8  9 10
                             11 12 13 14 15 16 17 18 19 20 21 22
                             23 24 25 26 27 28 29 30 31 32 33 34 35 36 37 38 39
                             40 41 42 43
                             44 45 46 47 48 49 50 51 52 53 54 55 56 57 58 59 60 61 62
                             63 64 65 66 67'
     new_ids             = '1 1 1   1 1 1   1 1 1   1 1 1   1 1 1   1 1 1   1 1 1   1 1 1   1 1 1
1 1 1   1 1 1
                            2 2 3   2 2 3   2 2 3   2 2 3   2 2 3   2 2 3   2 2 3   2 2 3   2 2 3
```

```
2 2 3   2 2 3   2 2 3   2 2 3
                            4 2 3   4 2 3   4 2 3   4 2 3   4 2 3   4 2 3   4 2 3   4 2 3
4 2 3   4 2 3   4 2 3   4 2 3   4 2 3   4 2 3   4 2 3   4 2 3   4 2 3
                            3 2 3   3 2 3   3 2 3   3 2 3
                            5 2 3   5 2 3   5 2 3   5 2 3   5 2 3   5 2 3   5 2 3   5 2 3
5 2 3   5 2 3   5 2 3   5 2 3   5 2 3   5 2 3   5 2 3   5 2 3   5 2 3   5 2 3   5 2 3
                            6 6 6   6 6 6   6 6 6   6 6 6   6 6 6   6 6 6'
     layer_subdivisions  = ' 5 5 5 5 5 5 5 5 5 5
                             5 5 5 5 5 5 5 5 5 5 5 5
                             5 5 5 5 5 5 5 5 5 5 5 5 5 5 5 5 5
                             5 5 5 5
                             5 5 5 5 5 5 5 5 5 5 5 5 5 5 5 5 5 5 5
                             5 5 5 5 5 5'
     bottom_sideset      = 'bottom'
     top_sideset         = 'top'
   []
   [coarse_pin_cell]
     type = PolygonConcentricCircleMeshGenerator
     num_sides = 6
     polygon_size = 0.4567
     num_sectors_per_side = '2 2 2 2 2 2'
     background_block_ids = 1
     preserve_volumes = on
     quad_center_elements = true
   []
   [coarse_extrude]
     type                = NonuniformMeshExtruderGenerator
     input               = coarse_pin_cell
     extrusion_vector    = '0 0 1'
     layer_thickness     = '5.0 5.0 5.0 5.0 5.0 5.0 5.0 5.0 5.0 5.24
                            5.0 5.0 5.0 5.0 5.0 5.0 5.0 5.0 5.0 5.0 5.0 5.293
                            5.0 5.0 5.0 5.0 5.0 5.0 5.0 5.0 5.0 5.0 5.0 5.0 5.0 5.0 5.0 5.0 4.4108
                            5.0 5.0 5.0 4.7637
                            5.0 5.0 5.0 5.0 5.0 5.0 5.0 5.0 5.0 5.0 5.0 5.0 5.0 5.0 5.0 5.0 5.4 5.4
                            5.0 5.0 5.0 5.0 5.0 5.15'
     existing_subdomains = '1'
     layers              = '  0 1  2  3  4  5  6  7  8  9 10
                             11 12 13 14 15 16 17 18 19 20 21 22
                             23 24 25 26 27 28 29 30 31 32 33 34 35 36 37 38 39
                             40 41 42 43
                             44 45 46 47 48 49 50 51 52 53 54 55 56 57 58 59 60 61 62
                             63 64 65 66 67'
     new_ids             = '  1  2  3  4  5  6  7  8  9 10
                             11 12 13 14 15 16 17 18 19 20 21 22
                             23 24 25 26 27 28 29 30 31 32 33 34 35 36 37 38 39
                             40 41 42 43
                             44 45 46 47 48 49 50 51 52 53 54 55 56 57 58 59 60 61 62
                             63 64 65 66 67 68'
     layer_subdivisions  = ' 1 1 1 1 1 1 1 1 1 1
                             1 1 1 1 1 1 1 1 1 1 1 1
                             1 1 1 1 1 1 1 1 1 1 1 1 1 1 1 1 1
                             1 1 1 1
                             1 1 1 1 1 1 1 1 1 1 1 1 1 1 1 1 1 1 1
                             1 1 1 1 1 1'
     bottom_sideset      = 'bottom'
     top_sideset         = 'top'
   []
   [embed]
     type = CoarseMeshExtraElementIDGenerator
```

```
    input = extrude
    coarse_mesh = coarse_extrude
    coarse_mesh_extra_element_id = 'subdomain_id'
    extra_element_id_name = coarse_element_id
  []
  [scale]
    type = TransformGenerator
    input = embed
    transform = SCALE
    vector_value = '0.01 0.01 0.01'
  []
  [assign_material]
    type = SubdomainExtraElementIDGenerator
    input = scale
    subdomains = '1 2 3 4 5 6'
    extra_element_id_names = 'material_id'
    extra_element_ids = '1 2 3 4 5 6'
  []
[]
[GlobalParams]
  library_file = '../shift_09g/griffin-xs.xml'
  library_name = '3dpin'
  plus = true
  grid_names = 'Tfuel'
  grid = '1'
  isotopes    = 'pseudo'
  densities = '1.0'
  is_meter = true
  scalar_flux = 'flux_moment_g0_L0_M0 flux_moment_g1_L0_M0 flux_moment_g2_L0_M0 flux_moment_g3_L0_M0
[]

[TransportSystems]
  particle = neutron
  equation_type = eigenvalue
  G = 9
  ReflectingBoundary = '10000'
  VacuumBoundary = '10003 10004'
  [sn]
    scheme = DFEM-SN
    family = MONOMIAL
    order = FIRST
    AQtype = Gauss-Chebyshev
    n_delay_groups = 0
    NPolar = 3
    NAzmthl = 6
    NA = 0
    sweep_type = asynchronous_parallel_sweeper
    using_array_variable = true
    initialize_angular_flux = true
    collapse_scattering  = true
    hide_angular_flux = true
    hide_higher_flux_moment = 0
  []
[]

[AuxVariables]
  [nuFissionRR]
    order = FIRST
    family = L2_LAGRANGE
```

```
  []
[]

[AuxKernels]
  [nuFissionRR]
    type = VectorReactionRate
    block = '4'
    variable = nuFissionRR
    cross_section = nu_sigma_fission
  []
[]

[Materials]
  [Fuel]
    type = MixedMatIDNeutronicsMaterial
    block = '4'
  []

  [Nonfuel]
    type = MixedMatIDNeutronicsMaterial
    block = '1 2 3 5 6'
  []
[]

[Executioner]
  type = SweepUpdate
  verbose = false
  debug_richardson = true

  richardson_abs_tol = 1e-6
  richardson_rel_tol = 1e-5
  richardson_max_its = 100
  richardson_value = eigenvalue

  inner_solve_type = SI #GMRes
  max_inner_its = 8

  cmfd_acceleration = true
  coarse_element_id = coarse_element_id
  diffusion_eigen_solver_type = newton
  prolongation_type = multiplicative
  max_diffusion_coefficient = 0.2
[]

[Postprocessors]
  [nuFissionRR]
    type = ElementIntegralVariablePostprocessor
    block = '4'
    variable = nuFissionRR
  []
[]

[Outputs]
  csv = true
  exodus = true
  perf_graph = true
  [console]
    type = Console
    outlier_variable_norms = false
```

[]
[]

Table B.1. 90 intermediate-group energy bounds for reaction rate tallies with `Shift`.

Grp	Upper Energy (eV)	Grp	Upper Energy (eV)	Grp	Upper Energy (eV)	Grp	Upper Energy (eV)
1	1.419×10^{7}	26	3.877×10^{5}	51	9.119×10^{3}	76	4.785×10^{1}
2	1.179×10^{7}	27	3.337×10^{5}	52	7.849×10^{3}	77	3.051×10^{1}
3	9.802×10^{6}	28	2.873×10^{5}	53	6.755×10^{3}	78	1.945×10^{1}
4	8.147×10^{6}	29	2.472×10^{5}	54	5.814×10^{3}	79	1.241×10^{1}
5	6.771×10^{6}	30	2.128×10^{5}	55	5.005×10^{3}	80	7.910×10^{0}
6	5.627×10^{6}	31	1.832×10^{5}	56	4.307×10^{3}	81	5.043×10^{0}
7	4.677×10^{6}	32	1.576×10^{5}	57	3.707×10^{3}	82	1.357×10^{0}
8	3.887×10^{6}	33	1.357×10^{5}	58	3.191×10^{3}	83	3.649×10^{-1}
9	3.230×10^{6}	34	1.168×10^{5}	59	2.747×10^{3}	84	9.815×10^{-2}
10	2.685×10^{6}	35	1.005×10^{5}	60	2.364×10^{3}	85	2.640×10^{-2}
11	2.231×10^{6}	36	8.652×10^{4}	61	2.035×10^{3}	86	7.102×10^{-3}
12	2.019×10^{6}	37	7.447×10^{4}	62	1.751×10^{3}	87	1.910×10^{-3}
13	1.827×10^{6}	38	6.409×10^{4}	63	1.507×10^{3}	88	5.138×10^{-4}
14	1.653×10^{6}	39	5.517×10^{4}	64	1.297×10^{3}	89	1.382×10^{-4}
15	1.496×10^{6}	40	4.748×10^{4}	65	1.117×10^{3}	90	3.718×10^{-5}
16	1.353×10^{6}	41	4.087×10^{4}	66	9.611×10^{2}		
17	1.225×10^{6}	42	3.518×10^{4}	67	8.272×10^{2}		
18	1.108×10^{6}	43	3.028×10^{4}	68	7.120×10^{2}		
19	1.003×10^{6}	44	2.606×10^{4}	69	6.128×10^{2}		
20	9.072×10^{5}	45	2.243×10^{4}	70	5.275×10^{2}		
21	8.208×10^{5}	46	1.930×10^{4}	71	4.540×10^{2}		
22	7.065×10^{5}	47	1.662×10^{4}	72	2.895×10^{2}		
23	6.081×10^{5}	48	1.430×10^{4}	73	1.846×10^{2}		
24	5.234×10^{5}	49	1.231×10^{4}	74	1.177×10^{2}		
25	4.505×10^{5}	50	1.059×10^{4}	75	7.505×10^{1}		

Table B.2. 330 intermediate-group energy bounds for reaction rate tallies with `Shift`.

Grp	Upper Energy (eV)	Grp	Upper Energy (eV)	Grp	Upper Energy (eV)	Grp	Upper Energy (eV)
1	1.419×10^7	41	2.231×10^6	81	3.020×10^5	121	4.087×10^4
2	1.370×10^7	42	2.122×10^6	82	2.872×10^5	122	3.887×10^4
3	1.323×10^7	43	2.019×10^6	83	2.732×10^5	123	3.698×10^4
4	1.278×10^7	44	1.921×10^6	84	2.599×10^5	124	3.518×10^4
5	1.234×10^7	45	1.827×10^6	85	2.472×10^5	125	3.346×10^4
6	1.191×10^7	46	1.738×10^6	86	2.352×10^5	126	3.183×10^4
7	1.150×10^7	47	1.653×10^6	87	2.237×10^5	127	3.028×10^4
8	1.111×10^7	48	1.572×10^6	88	2.128×10^5	128	2.880×10^4
9	1.073×10^7	49	1.496×10^6	89	2.024×10^5	129	2.739×10^4
10	1.036×10^7	50	1.423×10^6	90	1.926×10^5	130	2.606×10^4
11	1.000×10^7	51	1.353×10^6	91	1.832×10^5	131	2.479×10^4
12	9.512×10^6	52	1.287×10^6	92	1.742×10^5	132	2.358×10^4
13	9.048×10^6	53	1.225×10^6	93	1.657×10^5	133	2.243×10^4
14	8.607×10^6	54	1.165×10^6	94	1.576×10^5	134	2.133×10^4
15	8.187×10^6	55	1.108×10^6	95	1.500×10^5	135	2.029×10^4
16	7.788×10^6	56	1.054×10^6	96	1.426×10^5	136	1.930×10^4
17	7.408×10^6	57	1.003×10^6	97	1.357×10^5	137	1.836×10^4
18	7.047×10^6	58	9.537×10^5	98	1.291×10^5	138	1.747×10^4
19	6.703×10^6	59	9.072×10^5	99	1.228×10^5	139	1.662×10^4
20	6.376×10^6	60	8.629×10^5	100	1.168×10^5	140	1.580×10^4
21	6.065×10^6	61	8.209×10^5	101	1.111×10^5	141	1.503×10^4
22	5.769×10^6	62	7.808×10^5	102	1.057×10^5	142	1.430×10^4
23	5.488×10^6	63	7.427×10^5	103	1.005×10^5	143	1.360×10^4
24	5.220×10^6	64	7.065×10^5	104	9.562×10^4	144	1.294×10^4
25	4.966×10^6	65	6.721×10^5	105	9.095×10^4	145	1.231×10^4
26	4.724×10^6	66	6.393×10^5	106	8.652×10^4	146	1.171×10^4
27	4.493×10^6	67	6.081×10^5	107	8.230×10^4	147	1.114×10^4
28	4.274×10^6	68	5.784×10^5	108	7.828×10^4	148	1.059×10^4
29	4.066×10^6	69	5.502×10^5	109	7.447×10^4	149	1.008×10^4
30	3.867×10^6	70	5.234×10^5	110	7.083×10^4	150	9.586×10^3
31	3.679×10^6	71	4.979×10^5	111	6.738×10^4	151	9.119×10^3
32	3.499×10^6	72	4.736×10^5	112	6.409×10^4	152	8.674×10^3
33	3.329×10^6	73	4.505×10^5	113	6.097×10^4	153	8.251×10^3
34	3.166×10^6	74	4.285×10^5	114	5.799×10^4	154	7.849×10^3
35	3.012×10^6	75	4.076×10^5	115	5.517×10^4	155	7.466×10^3
36	2.865×10^6	76	3.877×10^5	116	5.248×10^4	156	7.102×10^3
37	2.725×10^6	77	3.688×10^5	117	4.992×10^4	157	6.755×10^3
38	2.592×10^6	78	3.508×10^5	118	4.748×10^4	158	6.426×10^3
39	2.466×10^6	79	3.337×10^5	119	4.517×10^4	159	6.112×10^3
40	2.346×10^6	80	3.175×10^5	120	4.296×10^4	160	5.814×10^3

Table B.3. 330 intermediate-group energy bounds for reaction rate tallies with `Shift` (continued).

Grp	Upper Energy (eV)	Grp	Upper Energy (eV)	Grp	Upper Energy (eV)	Grp	Upper Energy (eV)
161	5.531×10^{3}	201	7.485×10^{2}	241	1.013×10^{2}	281	1.371×10^{1}
162	5.261×10^{3}	202	7.120×10^{2}	242	9.636×10^{1}	282	1.304×10^{1}
163	5.004×10^{3}	203	6.773×10^{2}	243	9.166×10^{1}	283	1.241×10^{1}
164	4.760×10^{3}	204	6.443×10^{2}	244	8.719×10^{1}	284	1.180×10^{1}
165	4.528×10^{3}	205	6.128×10^{2}	245	8.294×10^{1}	285	1.122×10^{1}
166	4.307×10^{3}	206	5.829×10^{2}	246	7.889×10^{1}	286	1.068×10^{1}
167	4.097×10^{3}	207	5.545×10^{2}	247	7.505×10^{1}	287	1.016×10^{1}
168	3.897×10^{3}	208	5.275×10^{2}	248	7.139×10^{1}	288	9.661×10^{0}
169	3.707×10^{3}	209	5.017×10^{2}	249	6.790×10^{1}	289	9.190×10^{0}
170	3.527×10^{3}	210	4.773×10^{2}	250	6.459×10^{1}	290	8.742×10^{0}
171	3.355×10^{3}	211	4.540×10^{2}	251	6.144×10^{1}	291	8.315×10^{0}
172	3.191×10^{3}	212	4.319×10^{2}	252	5.845×10^{1}	292	7.714×10^{0}
173	3.035×10^{3}	213	4.108×10^{2}	253	5.560×10^{1}	293	7.157×10^{0}
174	2.887×10^{3}	214	3.908×10^{2}	254	5.288×10^{1}	294	6.640×10^{0}
175	2.747×10^{3}	215	3.717×10^{2}	255	5.030×10^{1}	295	6.160×10^{0}
176	2.613×10^{3}	216	3.536×10^{2}	256	4.785×10^{1}	296	5.715×10^{0}
177	2.485×10^{3}	217	3.363×10^{2}	257	4.552×10^{1}	297	5.302×10^{0}
178	2.364×10^{3}	218	3.199×10^{2}	258	4.330×10^{1}	298	4.919×10^{0}
179	2.249×10^{3}	219	3.043×10^{2}	259	4.119×10^{1}	299	4.564×10^{0}
180	2.139×10^{3}	220	2.895×10^{2}	260	3.918×10^{1}	300	4.234×10^{0}
181	2.035×10^{3}	221	2.754×10^{2}	261	3.727×10^{1}	301	3.928×10^{0}
182	1.935×10^{3}	222	2.619×10^{2}	262	3.545×10^{1}	302	3.216×10^{0}
183	1.841×10^{3}	223	2.492×10^{2}	263	3.372×10^{1}	303	2.633×10^{0}
184	1.751×10^{3}	224	2.370×10^{2}	264	3.208×10^{1}	304	2.156×10^{0}
185	1.666×10^{3}	225	2.254×10^{2}	265	3.051×10^{1}	305	1.765×10^{0}
186	1.585×10^{3}	226	2.145×10^{2}	266	2.902×10^{1}	306	1.445×10^{0}
187	1.507×10^{3}	227	2.040×10^{2}	267	2.761×10^{1}	307	1.183×10^{0}
188	1.434×10^{3}	228	1.940×10^{2}	268	2.626×10^{1}	308	9.686×10^{-1}
189	1.364×10^{3}	229	1.846×10^{2}	269	2.498×10^{1}	309	7.930×10^{-1}
190	1.297×10^{3}	230	1.756×10^{2}	270	2.376×10^{1}	310	6.493×10^{-1}
191	1.234×10^{3}	231	1.670×10^{2}	271	2.260×10^{1}	311	5.316×10^{-1}
192	1.174×10^{3}	232	1.589×10^{2}	272	2.150×10^{1}	312	5.189×10^{-1}
193	1.117×10^{3}	233	1.511×10^{2}	273	2.045×10^{1}	313	5.065×10^{-1}
194	1.062×10^{3}	234	1.438×10^{2}	274	1.945×10^{1}	314	4.944×10^{-1}
195	1.010×10^{3}	235	1.367×10^{2}	275	1.851×10^{1}	315	4.826×10^{-1}
196	9.611×10^{2}	236	1.301×10^{2}	276	1.760×10^{1}	316	4.711×10^{-1}
197	9.142×10^{2}	237	1.237×10^{2}	277	1.675×10^{1}	317	4.598×10^{-1}
198	8.697×10^{2}	238	1.177×10^{2}	278	1.593×10^{1}	318	4.488×10^{-1}
199	8.272×10^{2}	239	1.120×10^{2}	279	1.515×10^{1}	319	4.381×10^{-1}
200	7.869×10^{2}	240	1.065×10^{2}	280	1.441×10^{1}	320	4.277×10^{-1}

Table B.4. 330 intermediate-group energy bounds for reaction rate tallies with `Shift` (continued further).

Grp	Upper Energy (eV)	Grp	Upper Energy (eV)	Grp	Upper Energy (eV)	Grp	Upper Energy (eV)
321	4.175×10^{-1}	324	1.716×10^{-2}	327	7.051×10^{-4}	330	2.898×10^{-5}
322	1.441×10^{-1}	325	5.921×10^{-3}	328	2.433×10^{-4}		
323	4.972×10^{-2}	326	2.043×10^{-3}	329	8.397×10^{-5}		